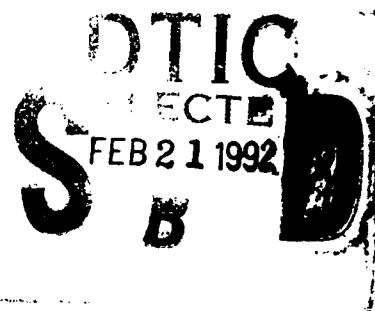


AD-A246 248



**NAVAL POSTGRADUATE SCHOOL**  
**Monterey, California**

2



**THESIS**

DEVELOPMENT OF AN ACTIVE DAMPING  
SYSTEM TO AID IN THE ATTITUDE  
CONTROL OF FLEXIBLE SPACECRAFT

by

Evan S. Jones

December, 1991

Thesis Advisor:

Prof. Brij N. Agrawal

Approved for public release; distribution is unlimited.

92 2 19 035

92-04381

UNCLASSIFIED

SECURITY CLASSIFICATION OF THIS PAGE

REPORT DOCUMENTATION PAGE				
1a REPORT SECURITY CLASSIFICATION Unclassified			1b RESTRICTIVE MARKINGS	
2a SECURITY CLASSIFICATION AUTHORITY			3 DISTRIBUTION/AVAILABILITY OF REPORT Approved for public release; distribution is unlimited.	
2b DECLASSIFICATION/DOWNGRADING SCHEDULE				
4 PERFORMING ORGANIZATION REPORT NUMBER(S)			5 MONITORING ORGANIZATION REPORT NUMBER(S)	
6a. NAME OF PERFORMING ORGANIZATION Naval Postgraduate School		6b OFFICE SYMBOL (If applicable) 55		7a NAME OF MONITORING ORGANIZATION Naval Postgraduate School
6c ADDRESS (City, State, and ZIP Code) Monterey, CA 93943-5000			7b ADDRESS (City, State, and ZIP Code) Monterey, CA 93943-5000	
8a NAME OF FUNDING/SPONSORING ORGANIZATION		8b OFFICE SYMBOL (If applicable)		9 PROCUREMENT INSTRUMENT IDENTIFICATION NUMBER
8c ADDRESS (City, State, and ZIP Code)			10 SOURCE OF FUNDING NUMBERS	
			Program Element No	Project No
			Task No	Work Unit Accession Number
11 TITLE (Include Security Classification) DEVELOPMENT OF AN ACTIVE DAMPING SYSTEM TO AID IN THE ATTITUDE CONTROL OF FLEXIBLE SPACECRAFT (UNCLASSIFIED)				
12 PERSONAL AUTHOR(S) Jones, Evan S.				
13a TYPE OF REPORT Master's Thesis		13b TIME COVERED From To		14 DATE OF REPORT (year, month, day) December 1991
15 PAGE COUNT 73				
16 SUPPLEMENTARY NOTATION The views expressed in this thesis are those of the author and do not reflect the official policy or position of the Department of Defense or the U.S. Government				
17 COSATI CODES			18 SUBJECT TERMS (continue on reverse if necessary and identify by block number)	
FIELD	GROUP	SUBGROUP	Spacecraft Attitude Control, Active Damping, Piezoceramics, Flexible Dynamics	
19 ABSTRACT (continue on reverse if necessary and identify by block number)  This thesis details the further refinement of the Naval Postgraduate School's Flexible Spacecraft Simulator and the first successful experimental control of the flexible system. The major emphasis of this work has been the development of a system to provide active damping to aid in control of the flexible modes of the system. The completed design of the circuit and the choice and placement of the piezoceramic sensors and actuators are presented. Verification of the computer model of the flexible system without active damping was completed and comparisons between the analytical and the experimental results are presented for simple proportional-derivative (PD) control using the main body angular position and rate.				
20 DISTRIBUTION/AVAILABILITY OF ABSTRACT <input checked="" type="checkbox"/> UNCLASSIFIED (N, M, etc.) <input type="checkbox"/> SAME AS REPORT <input type="checkbox"/> RESTRICTED			21 ABSTRACT SECURITY CLASSIFICATION Unclassified	
22a NAME OF RESPONSIBLE INDIVIDUAL Agrawal, Brij N			22b TELEPHONE (Include Area code) (408) 646 3338	22c OFFICE SYMBOL AA/Ag

DD FORM 1473, 84 MAR

83 APR edition may be used until exhausted  
All other editions are obsoleteSECURITY CLASSIFICATION OF THIS PAGE  
UNCLASSIFIED

Approved for public release; distribution is unlimited.

Development of an Active Damping  
System to aid in the Attitude  
Control of Flexible Spacecraft

by

Evan S. Jones  
Lieutenant, United States Navy  
B.G.S. Meteorology, University of Kansas, 1982

Submitted in partial fulfillment  
of the requirements for the degree of

MASTER OF SCIENCE IN ASTRONAUTICAL ENGINEERING

from the

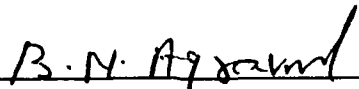
NAVAL POSTGRADUATE SCHOOL  
December, 1991

Author:



Evan S. Jones

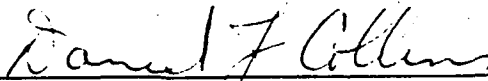
Approved by:



Brij N. Agrawal, Thesis Advisor



I. Michael Ross, Second Reader



Daniel J. Collins, Chairman,  
Department of Aeronautical and Astronautical Engineering

## ABSTRACT

This thesis details the further refinement of the Naval Postgraduate School's Flexible Spacecraft Simulator and the first successful experimental control of the flexible system. The major emphasis of this work has been the development of a system to provide active damping to aid in control of the flexible modes of the system. The completed design of the circuit and the choice and placement of the piezoceramic sensors and actuators are presented. Full operation of the completed damping system has not yet been achieved. Verification of the computer model of the flexible system without active damping was completed and comparisons between the analytical and the experimental results are presented for simple proportional-derivative (PD) control using the main body angular position and rate.



<b>Accession For</b>	
NTIS GRA&I	<input checked="checked" type="checkbox"/>
DTIC TAB	<input type="checkbox"/>
Unannounced	<input type="checkbox"/>
Justification	
By	
Distribution/	
Availability Codes	
Dist	Avail and/or Special
A-1	

## TABLE OF CONTENTS

I. INTRODUCTION .....	1
A. REASON FOR ANALYSIS .....	1
B. SCOPE OF THESIS .....	2
II. EXPERIMENTAL SETUP .....	4
A. SATELLITE MODEL .....	4
B. SENSORS .....	6
1. Main body sensors .....	6
2. Flexible arm sensors .....	6
C. ACTUATORS .....	11
1. Main body actuator .....	11
2. Flexible arm actuators .....	11
D. CONTROLLER .....	11
III. THEORETICAL ANALYSIS .....	13
A. PIEZOCERAMIC THEORY .....	13
B. PIEZOCERAMICS APPLIED TO ACTIVE DAMPING .....	15
1. Lateral mode sensor relationships .....	16

2.	Lateral mode actuator relationships . . . . .	19
3.	Damping circuit . . . . .	20
C.	EQUATIONS OF MOTION . . . . .	25
D.	DAMPING ESTIMATIONS . . . . .	33
E.	FINITE ELEMENT ANALYSIS OF FLEXIBLE ARM . . . . .	34
IV.	COMPARISON OF SIMULATED AND EXPERIMENTAL CONTROL . .	36
A.	MATHEMATICAL MODEL . . . . .	36
B.	SIMULATED PROPORTIONAL-DERIVATIVE CONTROL . . . . .	36
C.	EXPERIMENTAL PROPORTIONAL-DERIVATIVE CONTROL . .	43
VI.	CONCLUSIONS . . . . .	51
A.	RECOMMENDATIONS FOR FURTHER STUDY . . . . .	52
APPENDIX A	. . . . .	53
APPENDIX B	. . . . .	54
A.	MSC/PAL 2 FINITE ELEMENT MODEL . . . . .	54
B.	FLEXIBLE ARM MODE SHAPES AND FREQUENCIES . . . . .	56
APPENDIX C	. . . . .	59

REFERENCES .....	65
------------------	----

INITIAL DISTRIBUTION LIST .....	66
---------------------------------	----

## **I. INTRODUCTION**

### **A. REASON FOR ANALYSIS**

For military and civilian applications, the increasing demands for higher electrical power and increased capacity for communications and remote sensing necessitate the deployment of larger structures. Solar arrays and concentrators, large enough to deliver kilowatts (and even megawatts) of power for space based factories, large structures for phased array radar, as well as antennas for imaging the farthest reaches of the universe are but a few examples of the coming revolution in our use of space. Nevertheless, the prohibitive cost to launch and the limitations of current launch vehicle payload capability, require that the structures be designed with minimum mass. The result of these diverging design criteria is a class of structures with extremely low natural frequencies that can couple with the wide bandwidth of attitude control systems to greatly complicate meeting mission requirements (high pointing accuracy and high slew rates).

One interesting and promising tool to help overcome those potential control problems is the use of what has become known as "smart structures." In general, smart structures are elements of the system that are able to provide information about the dynamic state of the structure and/or change the structural properties as system demands change. Some examples of these are: composite structures with strain gages or small microphones, embedded as sensors, to give real time feed back of the integrity of the component; piezoelectric or shape metal memory actuators embedded in a structure to



act as actuators to control structural vibrations; and, fiber-optic sensors to provide real-time position and motion information. All of the aforementioned technologies have the potential to provide partial solutions to the complex problem of controlling large flexible structures.

One technology that is quite promising is the use of small piezoceramic sensors and actuators embedded in, or bonded along the structure to provide active damping of that structure. Though these devices require high voltages (in the hundreds of volts) to perform as actuators, they draw little current and so require minimal power. The nature of the system is that it provides damping to the structure when needed and its effect (and voltage requirement) is absent when not required. The purpose of this work is two fold: to verify the validity of the computer simulation of a simple proportional-derivative (PD) control system on the Flexible Spacecraft Simulator (FSS) and to develop a system that will eventually provide active damping to the FSS.

## **B. SCOPE OF THESIS**

This thesis details the initial operation of the FSS and the development of a system to increase the damping in the system. The FSS design and manufacture was detailed in Ward[Ref. 1] and Watkins[Ref. 2]. Previously, only simulations were performed to predict the response of the FSS to various inputs. This thesis seeks to verify the validity of those simulations by their comparison to experimental results. Impulse disturbance torque and slew maneuvers are simulated for the configuration. Plots showing simulated and experimental results are shown for the slew maneuver. Additionally a system will

be developed to use piezoceramic sensors and actuators to provide active damping to the flexible member of the FSS.

## II. EXPERIMENTAL SETUP

For a detailed explanation of the equipment and laboratory setup consult [Ref. 2].

The basic configuration of the experiment is shown in Figure 1.

### A. SATELLITE MODEL

Central to the FSS is a two dimensional spacecraft model that is suspended above a large granite table on a cushion of air. The "spacecraft" itself consists of a circular aluminum disk of 0.762 m diameter and 2.22 cm thickness and an L-shaped flexible

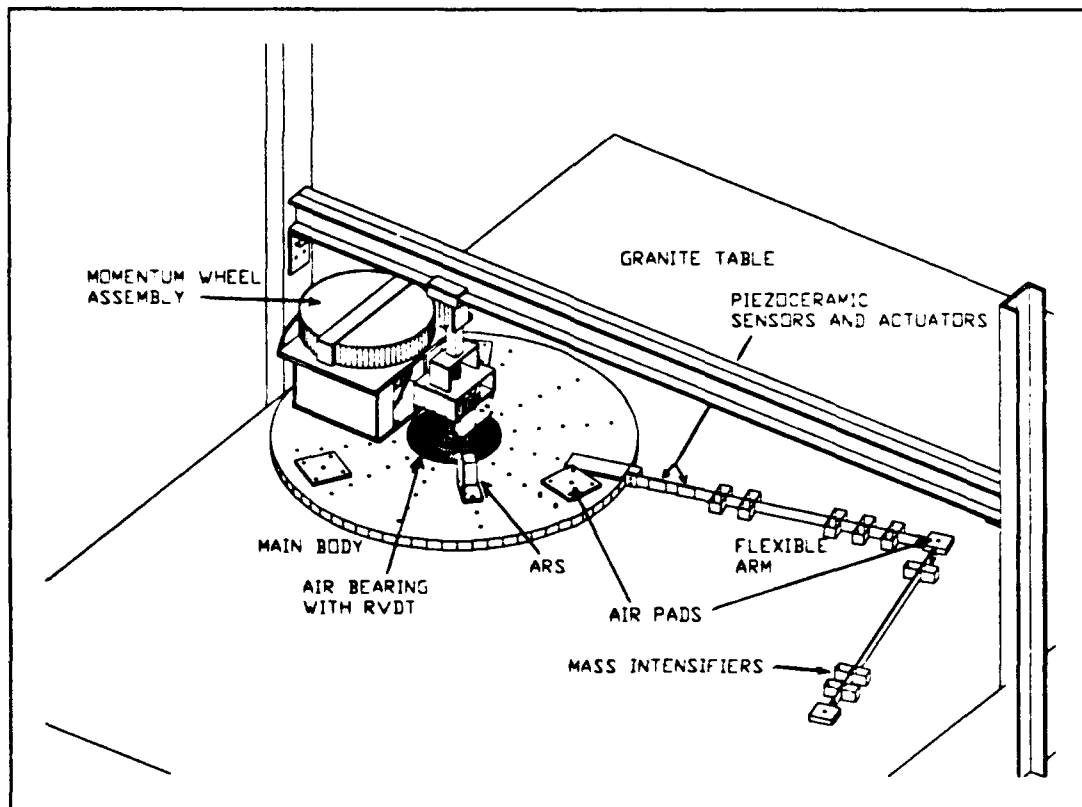


Figure 1 Flexible Spacecraft Simulator (FSS)

aluminum arm mounted radially outward. Each of these pieces is supported by small air pads which float just above the granite table. The central body is constrained to rotate about its center by an air bearing that is anchored to an overhead I-beam. The purpose of this configuration is to create a nearly frictionless environment in the two dimensions parallel to the plane of the motion of the model. The plane of motion is horizontal to eliminate gravitational effects.

The flexible arm is intended to simulate a large space structure with a fundamental frequency of around 0.10 Hz. In order to accomplish this in the limited space offered by the 6 ft by 8 ft granite table, the low frequency was achieved by adding concentrated masses along the beam. When the arm is tailored with increased mass, the stiffness remains the same, and the system has modal frequencies associated with a much larger structure.

The wiring and tubing required for the sensors, actuators, air bearing and air pads are gathered at the top of the vertical support and pass down to the central body near the axis of rotation. This is necessary to minimize their stiffness effect on the FSS system. These components were chosen to be as flexible as possible, and the number of lines passing to the body were minimized. Nevertheless, even the small effect of their presence is noticeable in the control of the model. These effects will be addressed more thoroughly in Chapter V

## **B. SENSORS**

### **1. Main body sensors**

Body angular position and angular rate are sensed through one rotary variable differential transformer (RVDT), and an angular rate sensor (ARS), respectively. The RVDT is mounted along the rotational axis above the main body and the ARS is mounted on the top surface of the main body. Wheel speed information is measured by an analog tachometer that is integral to the motor that drives the momentum wheel.

### **2. Flexible arm sensors**

Two types of sensors are employed on the flexible arm. The first are strain gauges. Three 350  $\Omega$  strain gauges are connected in series and mounted side by side on the face of the flexible arm to provide data to experimentally determine the system damping. Their output is delivered to a strip chart recorder where the signal can be analyzed and measurements of strain amplitudes can be made. The gauges are connected in the above manner in order to amplify the output and make the signal easier to display on the recorder. This information is used to verify the strain state sensed by the piezoceramic sensors.

The second type of sensor is the Navy Type II piezoceramic wafer. Navy Type II piezoceramics are a highly stable lead zirconate titanate (PZT) ceramics. There are two 2.54 x 3.81 cm, 0.25 mm thick wafers bonded at the base of the flexible arm. Figure 2 shows their placement. Each wafer is attached to the face of the arm with a

combination of 3-M brand 9703, conductive adhesive transfer tape, and two part epoxy adhesive.

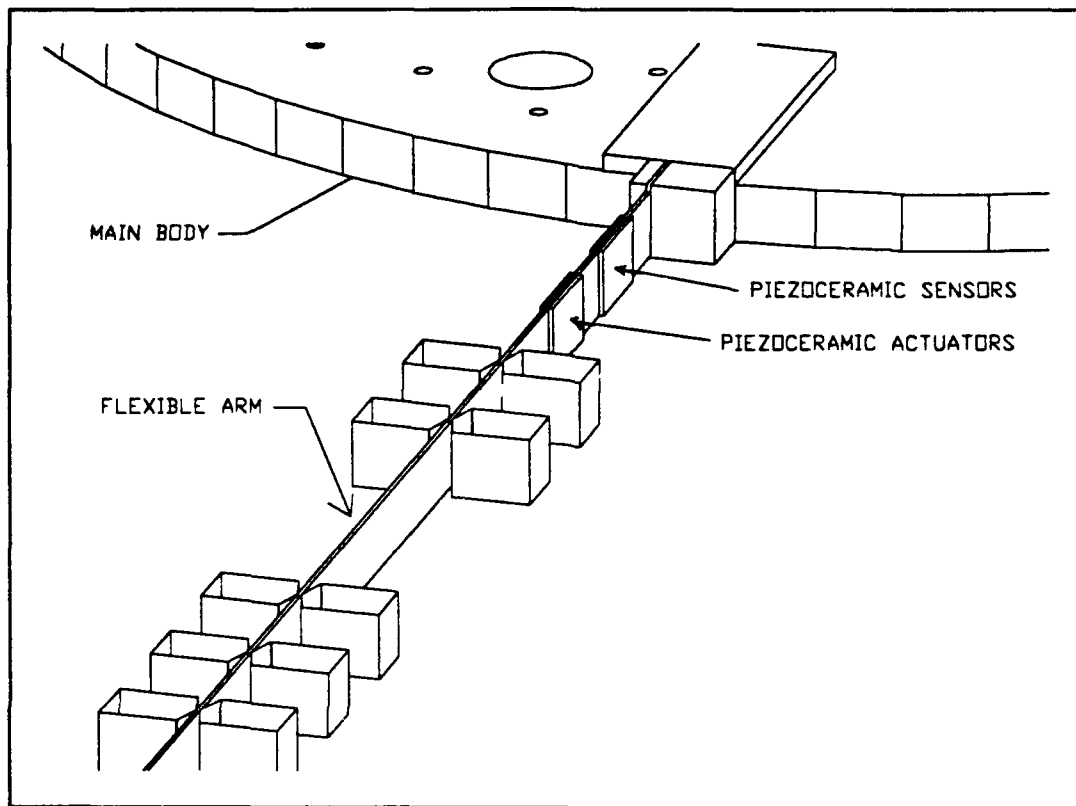


**Figure 2** Piezoceramic sensor and actuator placement

Many hours were devoted to developing the best method of adhering the piezo wafers. The biggest problem encountered was the difficulty in obtaining sufficient quantities of this material, in the correct dimensions to allow experimentation in attachment methods. Because of the brittle nature of the material, for the dimensions used for this research, great care must be used in even the most benign processing and handling environments. There appears to be only two ways to obtain the material. The first is to purchase the desired size and composition from the manufacture. All of this material is custom manufactured, and a minimum order would cost about \$1500.00 and

provide hundreds of the wafers. The second method is to obtain over-stocks of material manufactured for another organization. One must be prepared to be at the mercy of that supplier to deliver sufficient quantities of the wafers. The material for this research was donated by Phillips Laboratory at Edwards AFB. Unfortunately, they were only able to spare enough material to allow for the placement of two sensors and two actuators, with no spares. (When we damaged two of those original four, they were able to supply several replacements at the last minute.) No proven method existed to mount and electrically connect the wafers to the arm, so great care had to be used in developing those methods that would require only one opportunity with the wafers that were supplied.

The basic method of application requires that one side of each wafer be connected to a common ground while the other side be connected to the rest of the damping circuit. Because we have an aluminum arm as the mounting surface, one obvious method would seem to be to use that arm as the common ground. At first glance it seemed that using a conductive adhesive along the entire back face of the wafer would accomplish the desired results. However Dr Alan Bronowicki, staff scientist at TRW and co-author of Betros[Ref. 3], suggested that we would still need to insulate the edges of the wafer from the ground, because of the high voltages that could short across the actuating wafers (to be described in the next section). The second approach is to connect a grounding conductor, wire or foil, at a spot on the back of the wafer and insulate the entire piece from the arm. This method is the most straightforward, electrically.

The final method chosen, based upon much experimentation, made use of a conductive adhesive rather than a separate metallic conductor for several reasons. The first is the fact that the extra insulation required around the conductor would raise the wafer farther off the surface than should be required and would provide an area of stress concentration that could result in a crack of the piezo. The second, is that the use of adhesives alone would result in a much more uniform attachment to the aluminum beam.

Trial efforts were conducted with several types of transfer film, liquid and gel type adhesives on microscope cover glass (used to simulate the size and fragility of the piezoceramic material). The method selected produced mixed results. It appears that there is enough variability in either the material or the mounting geometry to cause the piezos to respond differently to similar strain. One of the actuators is able to produce approximately 8 volts when the elbow is deflected about eight centimeters from neutral. A similar deflection produces only a one to two volt response in the remaining piezos. Further investigation will be required to resolve this discrepancy.

Figure 3 shows the arrangement that was used. The wafer was first attached, outside face down, to a flat metal block with a thin layer of weak adhesive (accomplished by rubbing 3-M brand *Post-it*® on the block), providing a stable, flat surface to apply the epoxy and film adhesives and handle the fragile piezo wafers while mounting. Two small strips of conductive film adhesive, each 2 mil thick, were placed on top of one another near the center of the wafer aligned with the axis of the arm. Around that was spread a thin film of the epoxy adhesive. One more strip of conductive film adhesive was attached to the arm in order to provide a quick bond of the conductive portion of the



connection before the epoxy could flow over the film adhesive. The wafer was then applied to the arm with the metal block now resting on top to insure even application of the adhesives. The block was removed when the adhesive had spread out uniformly and was allowed to dry. After the adhesive had cured, the outside electrical connections were made by using the conductive film adhesive to connect wire leads to the center of the nickel electrode. Attempts were made to solder the wire to the nickel; however, since the joint was unsupported, the smallest pull on the wire was able to detach both the wire and the nickel electrode.

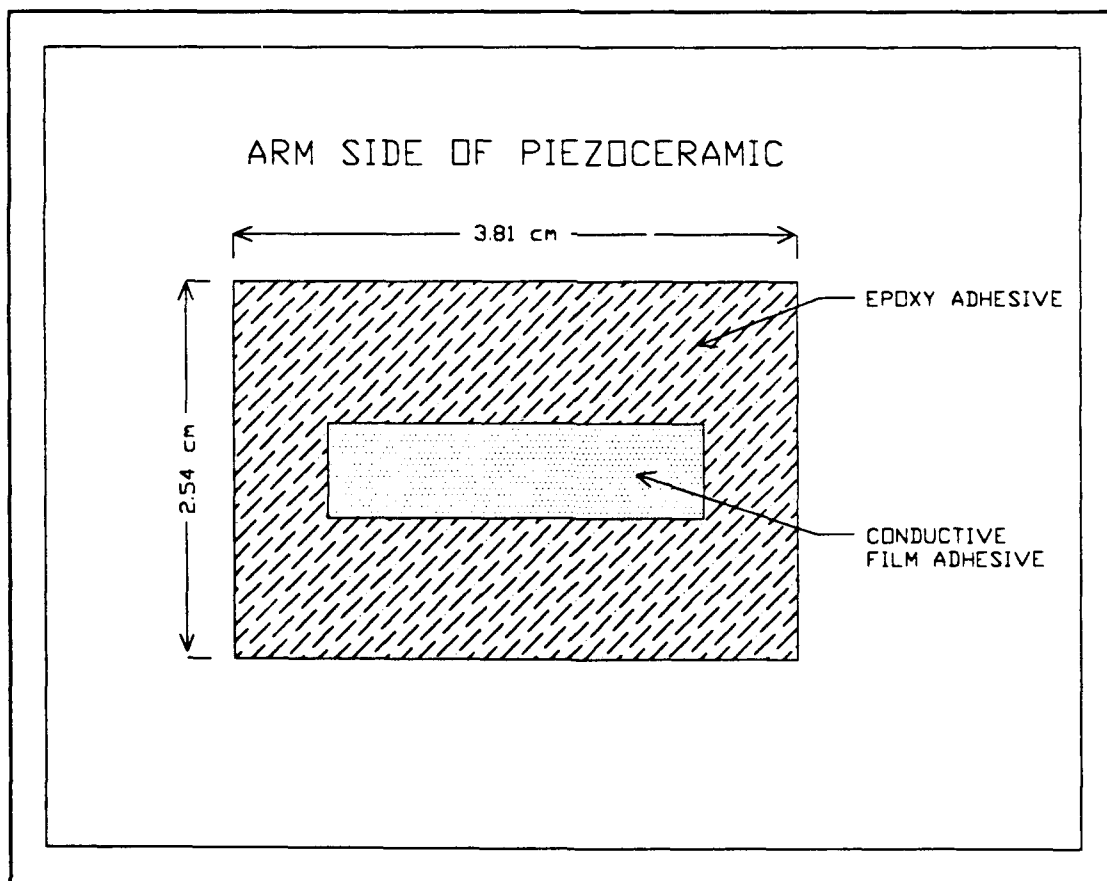


Figure 3. Piezo attachment method

## **C. ACTUATORS**

### **1. Main body actuator**

The single main body actuator is a 10.7 kg (26.16 cm diameter, 2.54 cm thick) steel disk attached to a 1.4 HP DC servo motor. This system acts as a biased momentum wheel assembly for control of the FSS in the two dimensional plane of the motion of the experiment. The entire assembly is mounted opposite to the flexible arm on the main body disk.

### **2. Flexible arm actuators**

The actuators for the flexible arm are piezoceramic wafers identical to the wafers that are used as sensors which were described earlier. The attachment method is the same as that of the sensors. They are located on opposite sides of the flexible arm, 5.7 cm outboard of the sensing wafers, (see Figure 2). The amplified output developed by the sensors, which results from the lateral strain in the arm, is applied to the actuating piezos in such a way that they are laterally strained in a direction opposite to the strain state in the arm. This has the effect of adding damping to the system.

## **D. CONTROLLER**

The FSS is controlled through the use a of software based controller manufactured by Integrated Systems, Inc. of Palo Alto, California. The software resides on a Digital Equipment, VAXStation 3100 model 30. This system provides the environment to

graphically design all components of the control system, simulate the response, and provide for real-time, interactive control of the actual system. Connected to the VAXStation is the AC-100 controller which is used to support the real-time control. It provides the processors and input/output devices need to control the momentum wheel and receive the sensor data for use in the control system.

### **III. THEORETICAL ANALYSIS**

#### **A. PIEZOCERAMIC THEORY**

Background for this section was gathered from the Vernitron Guide[Ref. 4] and [Ref. 3]. Piezoelectricity was first identified in the late 19th century by Pierre and Jacques Curie. They were the first to realize that some naturally occurring materials were able to couple electrical energy and mechanical energy. Certain crystal materials exhibit these useful properties: as a result of pressure applied to them, they produce a voltage potential between their faces; likewise, when an electrical field is applied across the material, a dimensional change occurs in the crystalline structure. It has been readily apparent to many scientists, since this discovery, the great potential the electric-to-mechanical coupling offers. In 1916, Paul Langevin developed the first practical and most enduring use of piezoelectricity, the sonar transducer and receiver, Shields[Ref. 5]. Langevin used naturally occurring quartz embedded between electrodes to transmit sound pulses, and a similar arrangement to detect the reflected energy. Although this effect occurs naturally in some materials like quartz, the greatest potential comes from man-made materials, since the material properties can be tailored to the specific application.

The materials used in this research are piezoceramics. They offer the advantage that, as ceramics, they can be machined into almost any shape and are largely chemically inert. It is during the manufacturing process that the material properties are tailored. As the ceramic material is being processed it is heated to a temperature above its Curie

point, and an electric field is applied. This results in an increase in the dimension along the axis parallel to the applied electric field and a decrease in the dimensions perpendicular to that axis, (see Figure 4). The axis parallel to the electric field defines the "poling" direction,  $\bar{P}$ , which can be oriented exactly to achieve the desired effect.

Piezoelectric devices are typically employed in one of two modes and the orientation of the poling axis is important in defining the electro-mechanical relationships for these modes. The first mode is the "motor" or actuator mode in which application of a voltage potential, less than the poling voltage, causes a deformation in the device. As an example, a voltage with polarity in the poling direction causes expansion of the ceramic along the axis parallel to the poling direction and contraction perpendicular to

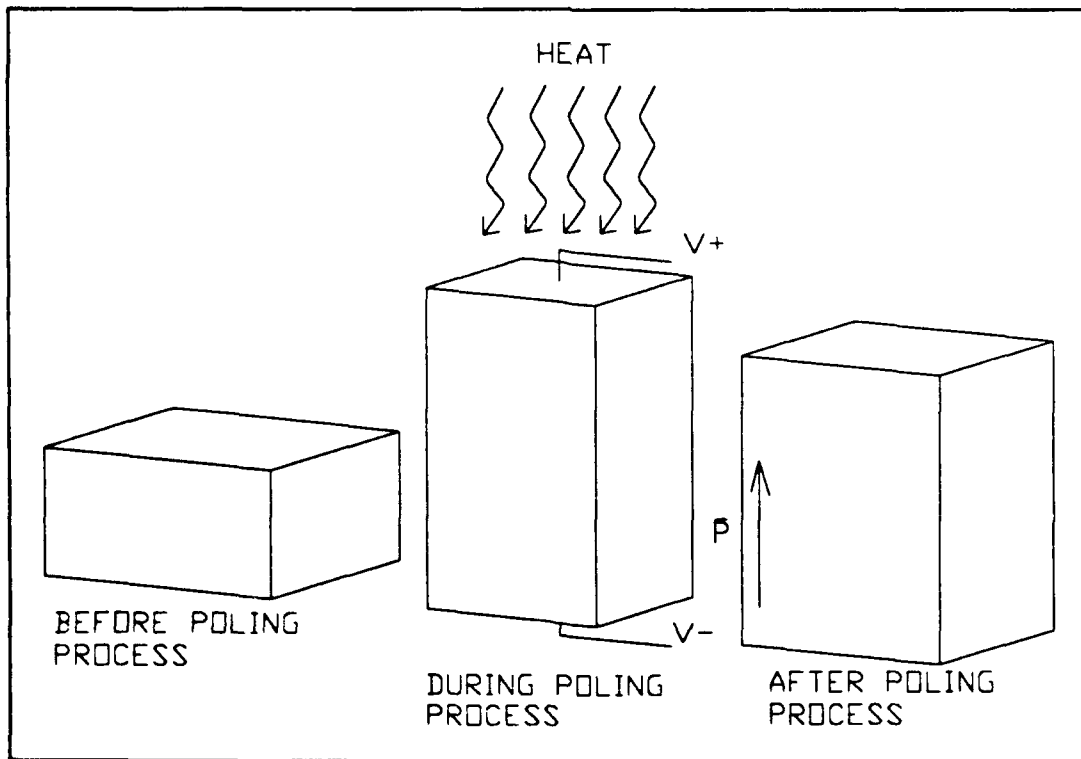


**Figure 4** Effects of poling process on piezoceramic

that axis. Application of a similar voltage with the opposite polarity causes contraction parallel to the poling axis and expansion perpendicular to it, (see Figure 5).

The second mode is the "generator" or sensor mode. In this case, a mechanical force applied to the device causes a proportional voltage to be developed across the faces of the device. As an example, a compressive force applied parallel to  $\vec{P}$  (or a tensile force applied perpendicular to  $\vec{P}$ ) causes a voltage to be developed that has the same

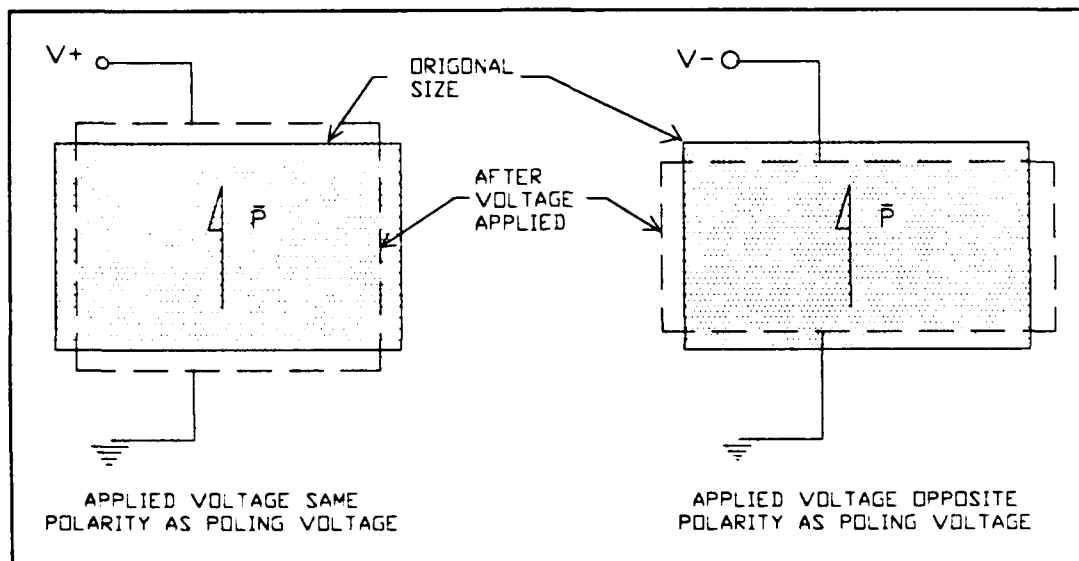


**Figure 5** Effects of applied voltage polarity

polarity as  $\vec{P}$ . The application of the opposite forces as above will thus develop voltages with opposite polarity to  $\vec{P}$ , (see Figure 6).

## **B. PIEZOCERAMICS APPLIED TO ACTIVE DAMPING**

The ability of the piezoceramic to couple electric and mechanical energy is the key to their utility in introducing active damping to a flexible system. The idea is to bond

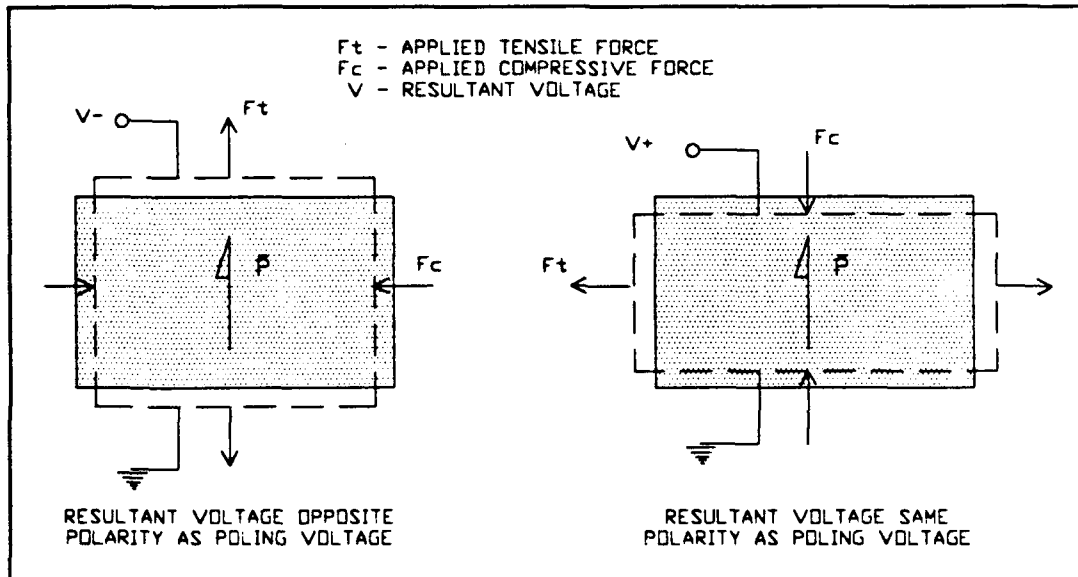


**Figure 6** Effects of applied forces on piezoceramic

the wafers to the surface of the flexible arm and provide the voltage developed from the sensors to the actuators in such a way that the actuators always attempt to oppose the motion of the arm. In this case, the piezo wafers are employed in the "lateral mode;" that is, they are mounted on the surface of the arm with their poling axes perpendicular to the mounting surface. The bending motion of the arm during slew maneuvers thus causes a lateral strain in the sensing piezos and application of a voltage across the actuating piezos results in a strain in the plane of bending that, if polarized correctly, will act to oppose the motion. Figure 7 shows the orientation of a piezoceramic wafer on the arm and the alignment of the axes that describe the electro-mechanical relationships.

### 1. Lateral mode sensor relationships

In the lateral mode, piezoceramic wafers, acting as sensors, will produce a charge between their electrode surfaces that is directly proportional to the strain across its lateral plane. This charge developed,  $Q$ , is described by the following relationship:

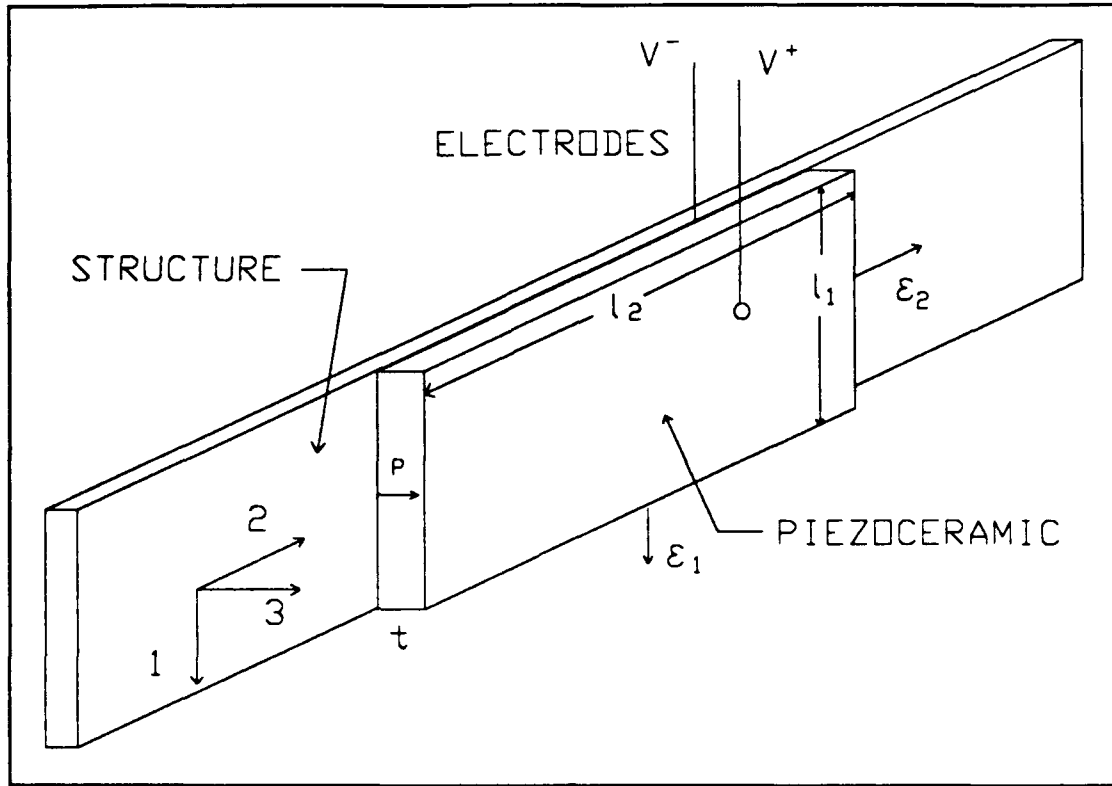


**Figure 7** Coordinate system for piezoelectric relationships

(the equations that follow in this section and the actuator section are from [Ref 3])

$$Q = A E d_{31} (\epsilon_1 + \epsilon_2) \quad (1)$$

where **A** is the lateral area of the piezo wafer, **E** is the Young's Modulus for the wafer, **d<sub>31</sub>** is the lateral charge coefficient (lateral strain / applied field), and  $\epsilon_1$  and  $\epsilon_2$  are the strain values in the lateral directions. The capacitance, **C**, of a piezoceramic wafer with the electrode arrangement shown in Figure 7 is given by

$$C = \frac{D A}{t} \quad (2)$$



where **D** is the dielectric constant of the piezoceramic and **t** is the thickness of the wafer.

Since voltage, **V**, is given by

$$V = \frac{Q}{C} \quad (3)$$

the voltage produced by the piezoceramic sensors is given by the relationship:

$$V = \left( \frac{E d_{31}}{D} \right) t (\epsilon_1 + \epsilon_2) \quad (4)$$

The following are properties of the Navy Type II PZT material used in this research:

**Table I NAVY TYPE II PZT PIEZOCERAMIC PROPERTIES**

---

Parameter	Description	Value	Units
<b>d<sub>31</sub></b>	Lateral strain coefficient	1.8 x 10 <sup>-10</sup>	meter/volt or coul/Newton
<b>E</b>	Young's Modulus	6.3 x 10 <sup>10</sup>	Pascal
<b>D</b>	Dielectric constant	1.5 x 10 <sup>-8</sup>	Farad/meter or Newton/volt <sup>2</sup>

---

The sensitivity of the piezoceramic sensor can then be estimated from these parameters and Equations (1), (2) and (3). For the Navy Type II wafers in this research, using the

dimensions given previously, the specific voltage developed,  $V_s$ , in units of volts/ $\mu$ -strain (where  $\mu$ -strain =  $\mu\text{m/m}$ ) is:

$$V_s = \frac{Q}{C} = 0.19 \left( \frac{\text{Volts}}{\mu\text{-strain}} \right) \quad (5)$$

As a comparison, a typical strain gage offers a sensitivity on the order of about 2  $\mu$ -Volts/ $\mu$ -strain, [Ref 3].

## 2. Lateral mode actuator relationships

When employing the piezoceramic wafers as actuators in the lateral mode, the attachment geometry is similar to the sensor geometry shown in Figure 7. The control voltage,  $V_c$ , is applied to the wafers and the lateral strain that is developed can act to control the bending of the beam. The electric field,  $\Phi$ , that is developed is given by

$$\Phi = \frac{V_c}{t} \quad (6)$$

Each piezoceramic material has a practical limit to the magnitude of the field that can be applied. Application of strong fields with opposite polarity to the poling direction can damage the material by depolarizing it. Typical field limits for most materials are between 500 and 1000 Volts/mm, [Ref 4]. The maximum free strain (i.e. for an unattached wafer) is given by:

$$\epsilon_{\max} = \Phi_{\max} d_{31} \quad (7)$$

For this damping circuit, the maximum control voltage was chosen to be  $\pm 175$  Volts, so the maximum free strain that can be developed is :  $\epsilon_{\max} = 124 \mu\text{-strains}$ . The maximum blocked stress (i.e. for a constrained piezo) is given by:

$$\sigma_{\max} = E \Phi_{\max} d_{31} \quad (8)$$

In this case, with the 175 Volt control voltage,  $\sigma_{\max} = 7.8\text{e}6 \text{ Pa}$ . These levels are for unattached wafers. When the piezoceramic is bonded to the arm the strain levels are reduced by the stiffness ratio, **SR**, given by:

$$\text{SR} = \frac{E_p t_p}{E_p t_p + E_s t_s} \quad (9)$$

So for the actuators on the arm of the FSS, the strain levels are reduced from  $124 \mu\text{-strains}$  to  $2.82 \mu\text{-strains}$ . It is apparent that the stiffer the actuator is in relation to the structure, the better an actuator it will be.

### 3. Damping circuit

The following circuit is based on the information contained in [Ref. 3] and on the great deal of help provided by Dr. Allen Bronowicki. The method of control used on the flexible arm is positive position feedback. This is obtained by feeding back structural position to a compensator and then feeding the compensator position multiplied by a gain back to the structure. The equations of motion that describe this method of control are:

$$\ddot{q}_s + 2 \zeta_s \omega_s \dot{q}_s + \omega_s^2 q_s = G \omega_s^2 q_c \quad (10)$$

for the arm, and

$$\ddot{q}_c + 2 \zeta_c \omega_c \dot{q}_c + \omega_c^2 q_c = \omega_c^2 q_s \quad (11)$$

for the compensator, where the  $q$ 's are the modal coordinates,  $\omega$ 's are fundamental frequencies,  $\zeta$ 's are damping ratios, and  $G$  is the gain applied to the feedback. The subscript "s" refers to the arm and the subscript "c" refers to the compensator.

The first section of the damping circuit is the charge amplifier. It takes the voltage developed in the piezo sensors and provides it as the input to a 15 Volt operational amplifier (op amp). The op amp then provides an output voltage based upon the relationship:

$$V_1 = -V_s \frac{C_s}{C_1} \quad (12)$$

where  $V_s$  is the voltage developed on the sensor, and the  $C$ 's are capacitors defined in Figure 8. The ratio of the capacitors in Equation (12) determine the gain of the sensing circuit. An initial gain of one was selected. Once the exact response of the sensors is determined, the final gain can be selected. The values of components of the circuits are shown in Table II. The sensing wafers are located on opposite sides of the arm with their poling directions aligned. Each piezo will sense the opposite strain state, but

provide the same polarity of signal, since the arm is acting as the ground. The values of  $C_1$  and  $R_1$  were selected to limit the D.C. response below a lower limit frequency,  $f_{ll}$ , that is much less than the fundamental frequency of the arm. For the values chosen, the lower limit frequency is 0.016 Hz, which is much less than the 0.138 Hz of the arm.

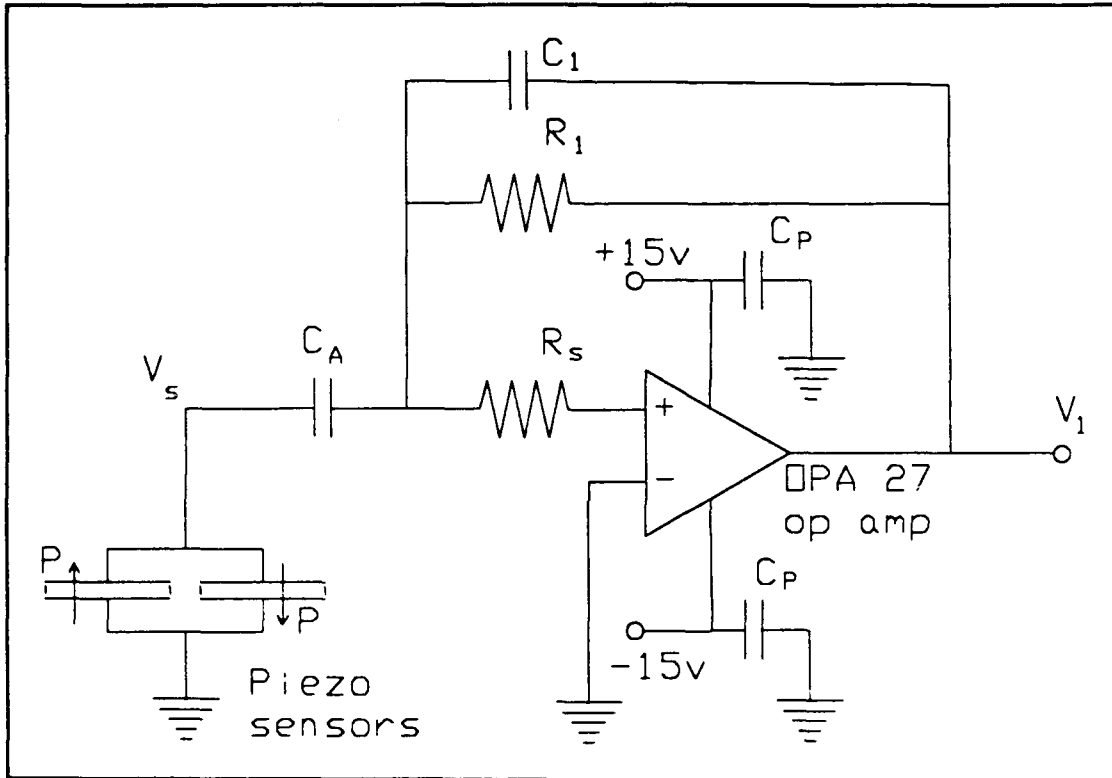


**Figure 8** Charge amplifier circuit

The next section of the circuit is the analog implementation of the compensator. The transfer function of the compensator is:

**Table II DAMPING CIRCUIT COMPONENTS**

ITEM	VALUE	ITEM	VALUE
$R_1$	$1M\Omega$	$C_1$	$1\mu F$
$R_2$	$1M\Omega$	$C_2$	$10\mu F$
$R_3$	$1M\Omega$	$C_3$	$0.1\mu F$
$R_4$	$20k\Omega$	$C_A$	$1\mu F$
$R_5$	$200k\Omega$	$C_P$	$0.1\mu F$
$R_5$	$500\Omega$		

$$H(s) = \frac{\omega_c^2}{s^2 + 2 \zeta_c \omega_c s + \omega_c^2} \quad (13)$$

which describes a second order low pass filter, (Figure 9). It employs a 15 Volt op amp and is designed around a cutoff frequency,  $f_c$  of 0.138 Hz (the measured fundamental frequency of the arm). The values of the capacitors and resistors in the circuit were sized to that frequency using the following relationships:

$$f_{lpr} = \frac{1}{2 \Pi} \left[ \frac{1}{R_2 R_3 C_2 C_3} \right]^{\frac{1}{2}} \quad (14)$$

and

$$\zeta_{lpr} = \left[ \frac{C_3 (R_2 + R_3)^2}{4 R_3 R_2} \right]^{\frac{1}{2}} \quad (15)$$

Using  $f_{lpr} = 0.15$  Hz and damping,  $\zeta_{lpr} = 0.1$ , the values of the components in the low pass filter were selected as listed in Table II.

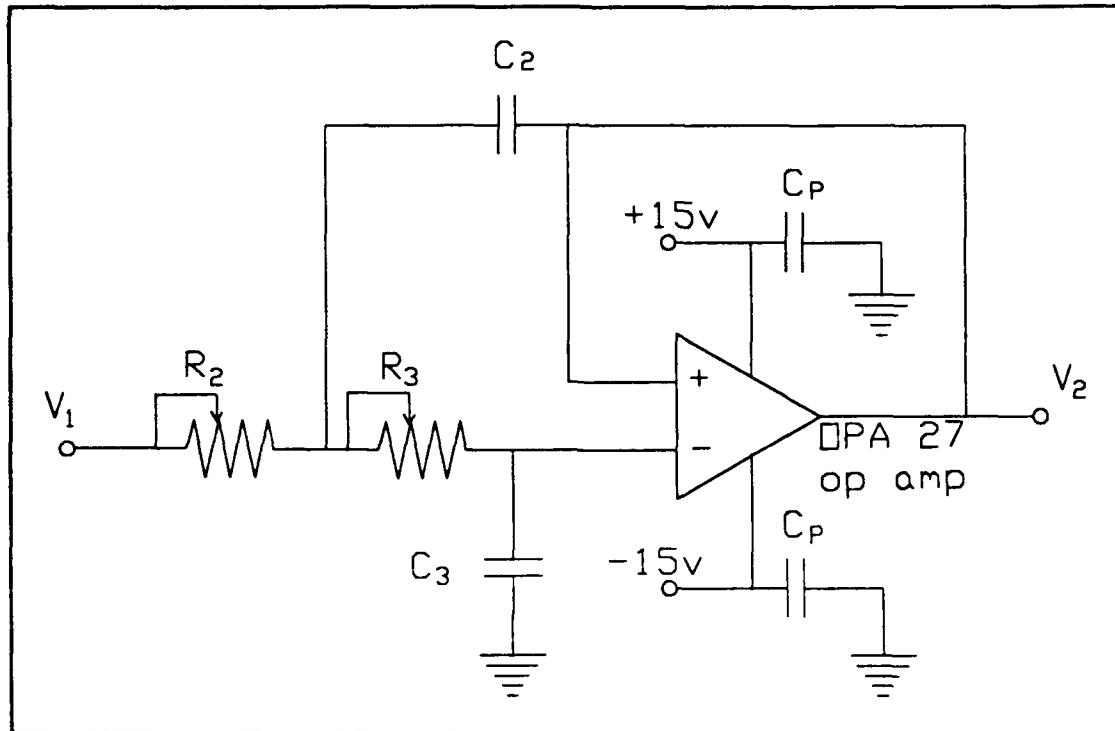


**Figure 9** Low pass filter

The final section of the circuit is the high voltage drive amp for the actuators (Figure 10). It is constructed around a  $\pm 175$  volt high power op amp (Apex Microtech PA-41 op amp) that provides the voltage to the piezoceramic actuators. The voltage provided to the actuators is determined by the following relationship:

$$V_3 = - V_2 \frac{R_s}{R_4} \quad (16)$$

where  $V_3$  is the voltage at the actuator,  $V_2$  is the voltage out of the low pass filter and  $R_4$  and  $R_s$  determine the gain of the amplifier. An initial gain of 10 was used to give the desired actuator voltage of 175 volts. This gain will eventually be tailored to the response of the actual sensors

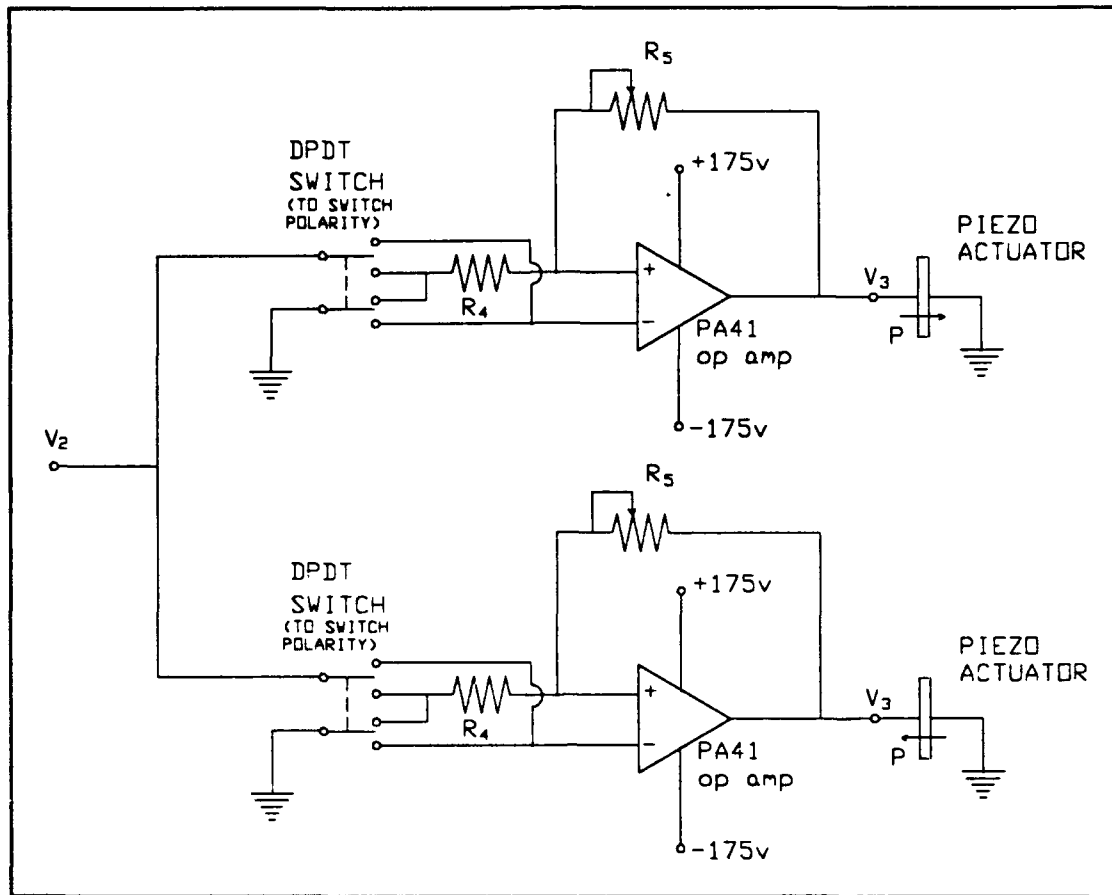


**Figure 10** Power amplification circuit

### C. EQUATIONS OF MOTION

The equations of motion for the system were fully derived in [Ref. 2] and are presented here for continuity. The hybrid-coordinate system illustrated in Figure Figure 11 is used in the derivation of the equations of motion. This splits the system components into rigid AND flexible bodies. The flexible bodies are assumed to be linearly elastic so that for small deformations, the elastic stresses remain proportional to the deformations. The flexible arm is further broken down into small rigid sub-bodies which correspond to concentrated masses or air pads under the arm. Lagrange's equation in this hybrid-coordinate system was used to derive the linearized equations of motion



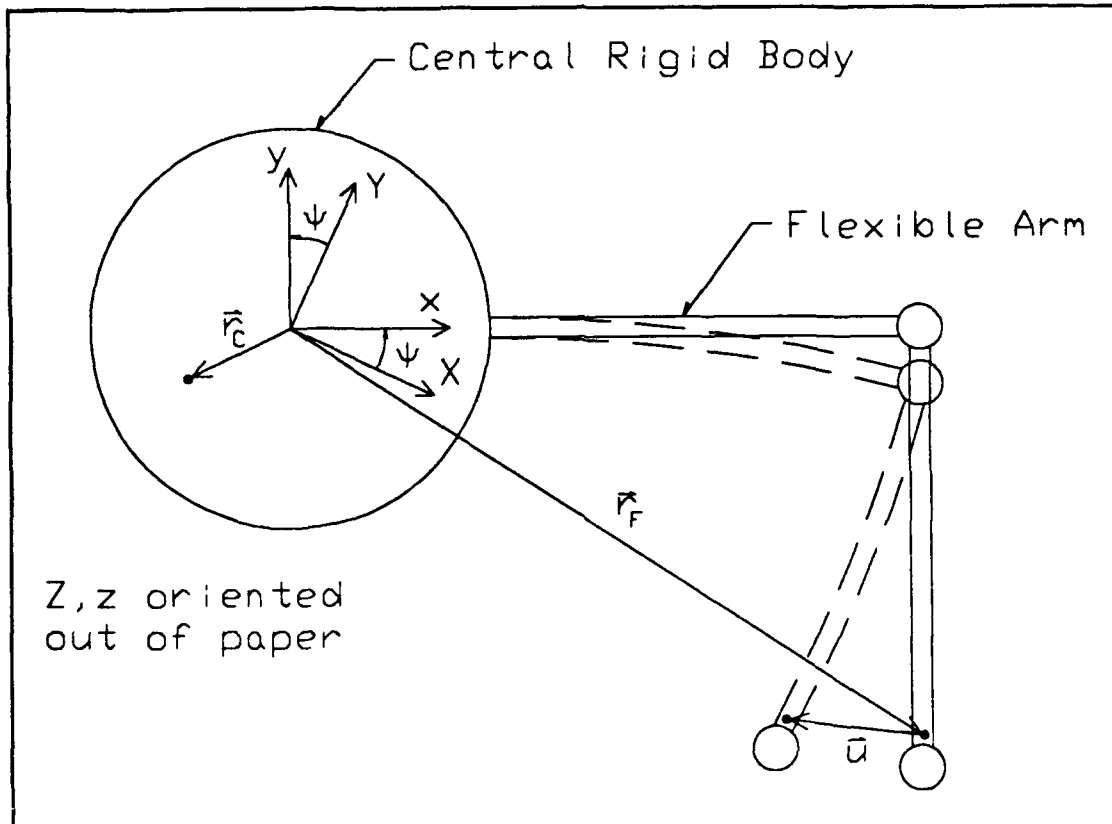


**Figure 11** Coordinate system for equations of motion

for the FSS. For these equations of motion, two coordinate systems were used. The first is the inertial coordinate system, centered at the pivot point of the main body. The second is the body coordinate system. It shares the same origin as the inertial coordinate system but rotates with the body. The angle that defines the relationship between the inertial and body coordinate systems is the rotation angle  $\Psi$ .

The first step in deriving the equations of motion is to determine the kinetic energy of the system. The kinetic energy,  $T$ , for the system is defined as:

$$T = \frac{1}{2} \int_C (\vec{V}_C \cdot \vec{V}_C) dm + \frac{1}{2} \int_F (\vec{V}_F \cdot \vec{V}_F) dm \quad (17)$$

where  $\vec{V}_C$  = velocity of a point on the central body

$\vec{V}_F$  = velocity of a point on the flexible body

The velocities are defined as:

$$\vec{V}_C = \dot{\Psi} \vec{k} \times \vec{r}_C \quad (20)$$

$$\vec{V}_F = \dot{\Psi} \vec{k} \times \vec{r}_F + \dot{\vec{u}} + \dot{\Psi} \vec{k} \times \vec{u} \quad (21)$$

where  $\vec{r}_C$  = position vector of a point on the central body

$\vec{u}$  = deformation vector of a point on the flexible body

$\vec{r}_F$  = position vector of a point on the undeformed arm

Substituting these velocities into Equation (17) gives

$$\begin{aligned}
T = & \frac{1}{2} \int_C \dot{\Psi}^2 (x_C^2 + y_C^2) dm + \frac{1}{2} \int_F [\dot{\Psi}^2 (x_F^2 + y_F^2) \\
& + (\dot{u}_x^2 + \dot{u}_y^2) + \dot{\Psi}^2 (u_x^2 + u_y^2) \\
& + 2\dot{\Psi} (x_H x_F \dot{u}_y - y_F \dot{u}_x) \\
& + 2\dot{\Psi}^2 (x_F u_x + y_F u_y)] dm
\end{aligned} \tag{25}$$

Neglecting the higher order terms and linearizing, we get the following equation in terms of the generalized coordinates  $\Psi$  and  $\mathbf{u}$

$$\begin{aligned}
T = & \frac{1}{2} I_{zz} \dot{\Psi}^2 + \frac{1}{2} \int_F (\dot{u}_x^2 + \dot{u}_y^2) dm \\
& + \dot{\Psi} \int_F (x_F \dot{u}_y - y_F \dot{u}_x) dm
\end{aligned} \tag{26}$$

where

$$I_{zz} = I_{zz}^C + I_{zz}^F = \int_C (x_C^2 + y_C^2) dm + \int_F (x_F^2 + y_F^2) dm \tag{27}$$

The generalized coordinate  $\mathbf{u}$  represents the elastic deformation of the modal coordinates of the flexible arm and is denoted by

$$\begin{aligned} u_x &= \sum_{i=1}^n \phi_i^x q_i(t) \\ u_y &= \sum_{i=1}^n \phi_i^y q_i(t) \end{aligned} \quad (28)$$

where the  $i$  subscript denotes the  $i$ th mode,  $q_i(t)$  is the modal coordinate,  $\phi_i^x$  is the component of the modal vector along the x-axis, and  $\phi_i^y$  is the component of the modal vector along the y-axis. Substituting these into Equation (26) gives

$$\begin{aligned} T &= \frac{1}{2} I_{zz} \dot{\Psi}^2 + \frac{1}{2} \int_F \left( \sum_{i=1}^n \sum_{j=1}^n [\phi_i^x \phi_j^x + \phi_i^y \phi_j^y] \dot{q}_i \dot{q}_j \right) dm \\ &\quad + \dot{\Psi} \int_F \left( x_F \sum_{i=1}^n \phi_i^y \dot{q}_i - y_F \sum_{i=1}^n \phi_i^x \dot{q}_i \right) dm \end{aligned} \quad (29)$$

If the modal masses are normalized and the orthogonality of the modal vectors is used, then Equation (29) becomes

$$T = \frac{1}{2} I_{zz} \dot{\Psi}^2 + \frac{1}{2} \sum_{i=1}^n \dot{q}_i^2 + \dot{\Psi} \sum D_i \dot{q}_i \quad (30)$$

where

$$\begin{aligned} D_i &= \int_F (x_F \phi_i^y - y_F \phi_i^x) dm \\ &= \text{rigid-elastic coupling.} \end{aligned} \quad (31)$$

Now the potential energy of the flexible system is

$$V = \frac{1}{2} \sum_{i=1}^n \omega_i^2 q_i^2 \quad (32)$$

where  $\omega_i$  is the frequency of the  $i$ th mode.

Lagrange's equation can then be applied as

$$\frac{d}{dt} \left( \frac{\partial L}{\partial \dot{\mu}_i} \right) - \frac{\partial L}{\partial \mu_i} = F_i \quad (33)$$

where

$$L = T - V \quad (34)$$

and  $\mu_i$  is the generalized coordinate and  $F_i$  is the generalized force. The generalized coordinates for this system are  $\Psi, q_1, \dots, q_n$ .  $F_1$  is equal to  $T$  and all other  $F_i$  equal zero. Substituting these into Equation (33) gives the equations of motion:

$$\begin{aligned} I_{zz} \ddot{\Psi} + \sum_{i=1}^n D_i \dot{q}_i &= T \\ \ddot{q}_i + \omega_i^2 q_i + D_i \dot{\Psi} &= 0 \end{aligned} \quad (35)$$

Introducing modal damping,  $\zeta_i$ , for the flexible arm, the equations of motion become

$$\begin{aligned}
I_z \ddot{\Psi} + \sum_{i=1}^n D_i \ddot{q}_i &= T \\
\ddot{q}_i + 2 \xi_i \omega_i \dot{q}_i + \omega_i^2 q_i + D_i \ddot{\Psi} &= 0
\end{aligned} \tag{36}$$

The equation of motion for the momentum wheel is

$$I_w \dot{\Omega} = -T \tag{37}$$

where  $I_w$  is the moment of inertia of the momentum wheel about its z-axis and  $\dot{\Omega}$  is the wheel rotation rate.

In order to implement these equations of motion in the AC-100 software controller, a state-space representation was constructed of the form:

$$\begin{aligned}
\dot{X} &= [A]X + [B]U \\
Y &= [C]X + [D]U
\end{aligned} \tag{38}$$

where  $X$  is a vector of state variables,  $U$  is the input vector and  $Y$  is the output vector:

$$\begin{aligned}
X &= [\Psi, q_1, \dots, q_n, \dot{\Psi}, \dot{q}_1, \dots, \dot{q}_n]^T \\
Y &= [\Psi, \dot{\Psi}]^T \\
U &= T \\
D &= 0 \\
B &= [0, 0, \dots, 0, 1, -D_1, \dots, -D_n]^T
\end{aligned} \tag{39}$$

and

$$A = \frac{1}{I_{zz}^0} \begin{bmatrix} 0 & 0 & \dots & 0 & I_{zz}^0 & 0 & \dots & 0 \\ 0 & 0 & \dots & 0 & 0 & I_{zz}^0 & \dots & 0 \\ \vdots & \vdots & & \vdots & \vdots & \vdots & & \vdots \\ 0 & F_1 & \dots & F_n & 0 & H_1 & \dots & H_n \\ 0 & -G_1 & \dots & -D_{iF_n} & 0 & J_1 & \dots & D_1 H_n \\ \vdots & \vdots & & \vdots & \vdots & \vdots & & \vdots \\ 0 & -D_{nF_1} & \dots & -G_n & 0 & -D_{nH_1} & \dots & -J_n \end{bmatrix} \quad (40)$$

where

$$\begin{aligned} I_{zz}^0 &= I_{zz} - \sum_{i=1}^n (D_i)^2 \\ F_i &= D_i \omega_i^2 \\ G_i &= \omega_i^2 I_{zz}^0 + D_i F_i \\ H_i &= 2\xi_i \omega_i D_i \\ J_i &= 2\xi_i \omega_i I_{zz}^0 + D_i H_i \end{aligned} \quad (41)$$

and finally

$$[C] = \begin{bmatrix} 1 & 0 & \dots & 0 & 0 & 0 & \dots & 0 \\ 0 & 0 & \dots & 0 & 1 & 0 & \dots & 0 \end{bmatrix} \quad (42)$$

#### D. DAMPING ESTIMATIONS

In order to accurately implement the system representation in the software controller and to verify the effect of the active damping system, it was necessary to experimentally determine the damping of the flexible arm. The method selected was the log decrement method. In this method the flexible body is deflected from some equilibrium position and released to freely vibrate. The amplitudes of the oscillations are measured and the number of cycles recorded. The damping may then be determined through the following formula:

$$\zeta = \frac{1}{2 \pi n} \ln \left[ \frac{X_i}{X_f} \right] \quad (43)$$

where  $X_i$  is the initial amplitude measured,  $X_f$  is the final amplitude measured and  $n$  is the number of cycles from the initial to the final measurement.

In this case, the strain in the arm was already of great interest and available through our sensors, the magnitude of the strain state in the arm was measured to determine the damping. Since the strain is proportional to the deflection of the arm and the sensors deliver a signal directly proportional to the strain, the output of the sensors could be used directly to measure the damping. As a check both strain gages and piezoceramics were used to initially verify the damping. The first effort was to mount a strain gage on the arm just outboard of the actuating piezos. The signal was then fed



to a strip chart recorder where the amplitude and cycle information could be read. Appendix A contains a sample printout of the strip chart. The difficult part of this evolution was to attempt to excite only one mode (the first), so that the amplitude measurements would be meaningful. This was accomplished through a lot of practice and allowing sufficient time for the higher modes to die out. Having conducted many runs of the process, the damping without the circuit active was found to be:  $\zeta = .004$ , or 0.40 % damping. The same method will be employed when the damping circuit becomes fully operational.

#### **E. FINITE ELEMENT ANALYSIS OF FLEXIBLE ARM**

In order to determine the state-space matrices, **A** and **B**, it was necessary to determine the frequencies and mode shapes of the flexible arm. This was most easily performed on a computer using a finite element analysis program to solve the complicated geometry. The MacNeal-Schwendler Corporation finite element software, MSC/pal 2, was used to do this analysis. It was selected because it is a PC based application and it's command structure is written in a "plain english" style.

The flexible arm was modeled as a 20 node uniform aluminum beam with mass elements located at the node locations corresponding to the locations of the mass intensifiers. The air pad bracket at the elbow and the end point were modeled as aluminum beams, .0254 m high, of sufficient thickness to give them the equivalent mass of the actual bracket. This method gave the bracket the correct mass and essentially no flexibility, as should be the case. The base of the beam, node 1, was constrained to have

translation or rotation. The remainder of the nodes were constrained to permit only **X** and **Y** translation and **Z** rotation. This resulted in a two dimensional fixed-free analysis. The model and results are contained in Appendix B.

## **IV. COMPARISON OF SIMULATED AND EXPERIMENTAL CONTROL**

### **A. MATHEMATICAL MODEL**

The form of the mathematical model (with the linearizations) implemented by Watkins in [Ref. 2] was used as a benchmark to continue the development of the FSS. The first six modes of the flexible arm were thought to be the most significant and were used in the creation of the state-space system. The fortran program FORME, (Appendix B), is a slightly modified version of the Watkins program FORM and was used with input from the finite element model to create the **A** and **B** matrices that describe the system dynamics. The measured structural damping of 0.4 % (without active damping) was used. These matrices were then discretized for use in the software simulation of the flexible system. The truncation of the modes after the first six appears to be a valid simplification as will be illustrated when the simulated and actual data are compared.

### **B. SIMULATED PROPORTIONAL-DERIVATIVE CONTROL**

The simple proportional-derivative control system for the FSS is based on feeding back the angular position,  $\Psi$ , and angular rate,  $\dot{\Psi}$ , of the rigid central body. Future plans call for feeding back the information supplied by piezoceramic sensors placed along the arm, however at this time they are intended only to be used for active damping of the system. Previous work performed by Watkins seemed to suggest that the arm is the critical component in the success any control system might have. Control gains that

would quickly reposition the FSS, might unacceptably deform the arm, perhaps to the point of destruction. (This was verified during the first attempts at controlling the actual FSS when spurious control torque signals caused the body rate to increase rapidly and permanently bend the arm.) The control law for the PD system is:

$$U = T_w = - ( K_1 \dot{\Psi} + K_2 \Psi ) \quad (44)$$

The gains,  $K_1$  and  $K_2$ , were set using pole placement methods for a rigid body ( $1/s^2$ ) plant. The control frequency selected,  $\omega_{pdc}$ , was 0.06 Hz and control system damping ratio,  $\zeta_{pdc}$ , was 0.9. The resulting gains were calculated to be:

$$\begin{aligned} K_1 &= 5.2553 \\ K_2 &= 1.3985 \end{aligned} \quad (45)$$

It became apparent that the control law for the analytical model required modification. During the first attempts to control the experimental model, it was discovered that the momentum wheel would continue to speed up even after the body reached its equilibrium position. This fact seemed to indicate the existence of some constant external torque acting on the body. One possibility was that the granite table was out of level and the body was seeking the lowest gravitational potential energy. The granite table was re-leveled, however, and the results did not change. After some consideration it became apparent that the many tubes and wires that were passed to the central body were creating a disturbance torque on the body. A number of the air hoses passing to the main body were consolidated and the remaining wires were repositioned to minimize their effect, but the disturbance could not be decreased to a point that its

effect was negligible. As a result, a model of the disturbance torque was added to the simulation to bring the model into closer agreement with the FSS.

As a first estimation, the disturbance torque was assumed to be constant. A plot of the actual momentum wheel speed was used to determine the magnitude of the added torque. The slope of the wheel speed vs time curve was measured. Since that slope represents acceleration, multiplying by the moment of inertia of the wheel results in torque. The disturbance torque,  $T_D$ , was estimated to be 0.016 N-m. This value is added into the control law which becomes

$$U = T_w = -(K_1 \dot{\Psi} + K_2 \Psi) + T_D \quad (46)$$

Slew and impulse maneuvers were simulated with these control system parameters, and the results are illustrated in Figure 12 and Figure 13. Each graph contains four sections showing the speed of the momentum wheel (in RPM), the torque produced by the momentum wheel (in N-m), the body position,  $\Psi$ , (in degrees), and the body rate,  $\dot{\Psi}$ , (in degrees/sec). Figure 14 and Figure 15 show the relative modal amplitudes for the 30 degree slew maneuver and impulses disturbance.

The results from the 30 degree slew maneuver show that the body responds quickly and approaches the new position in about 15 seconds. The body then settles out to the new position within about 20 to 25 seconds. The maneuver is a very controlled operation. The plot of the modal amplitudes indicates that the first mode is dominant, the second is much less important than the first, and the third through the sixth are almost nonexistent. It appears that the arm would have no problem sustaining this

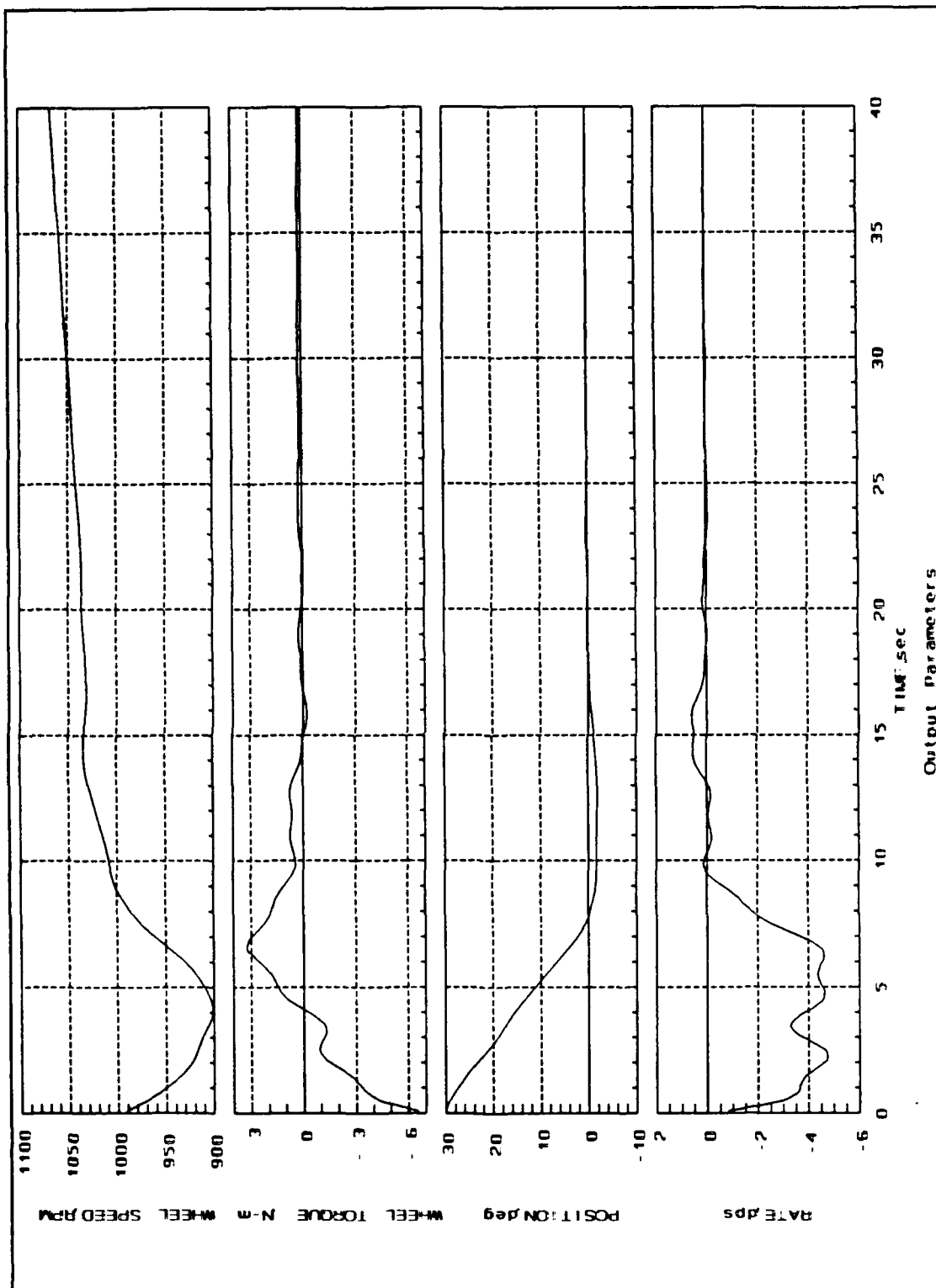


Figure 12 Simulated 30 degree slew maneuver

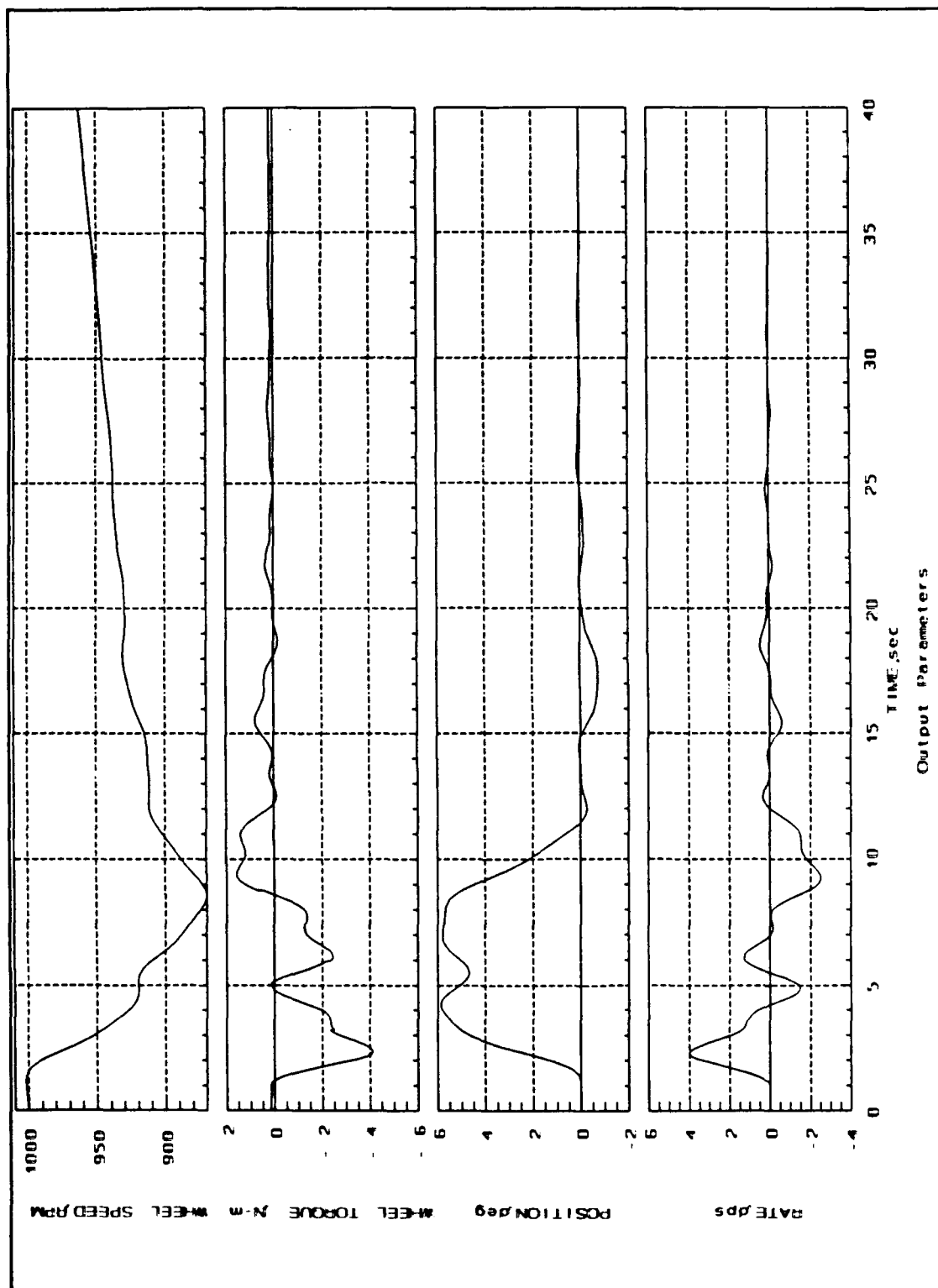
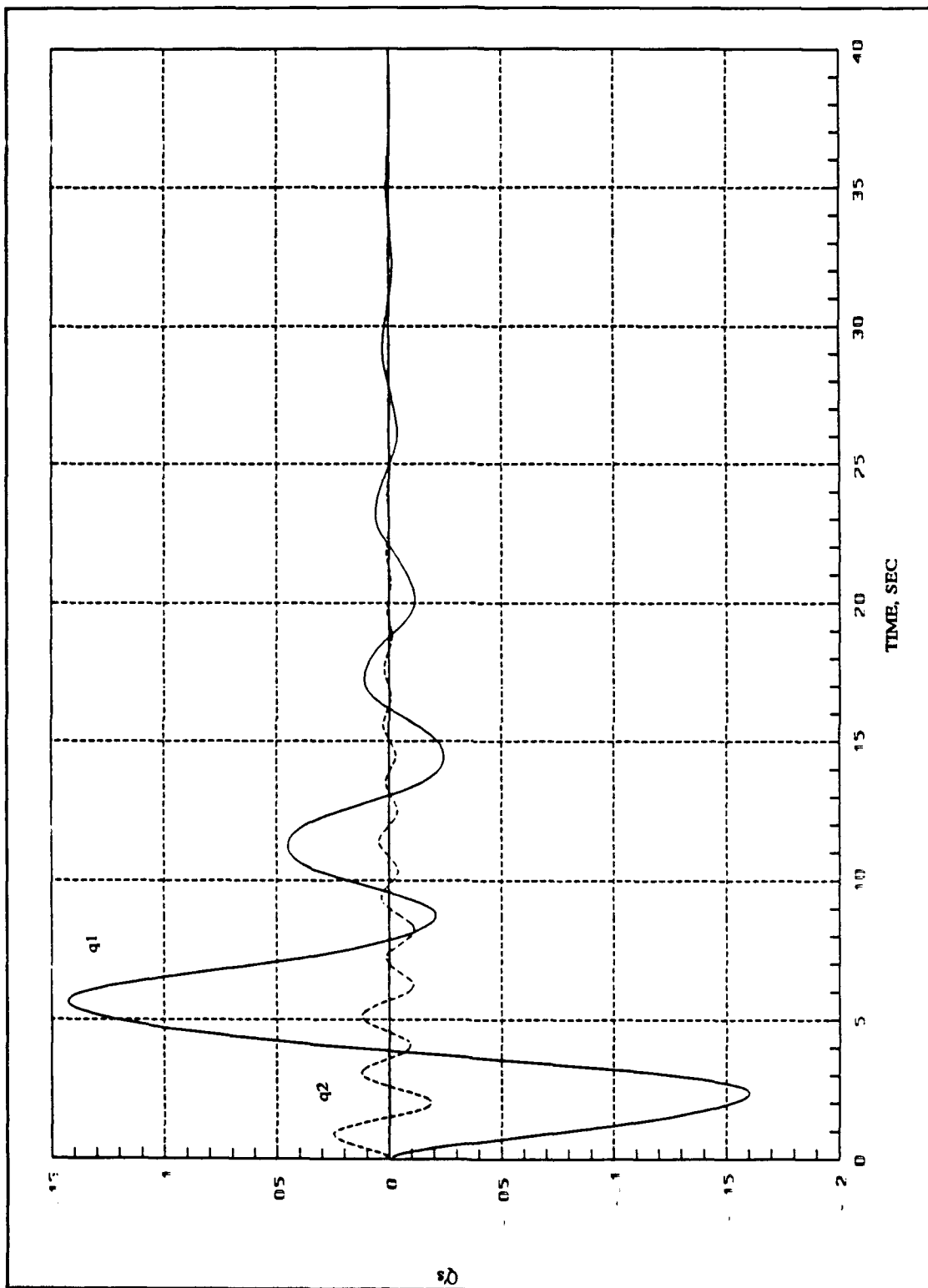
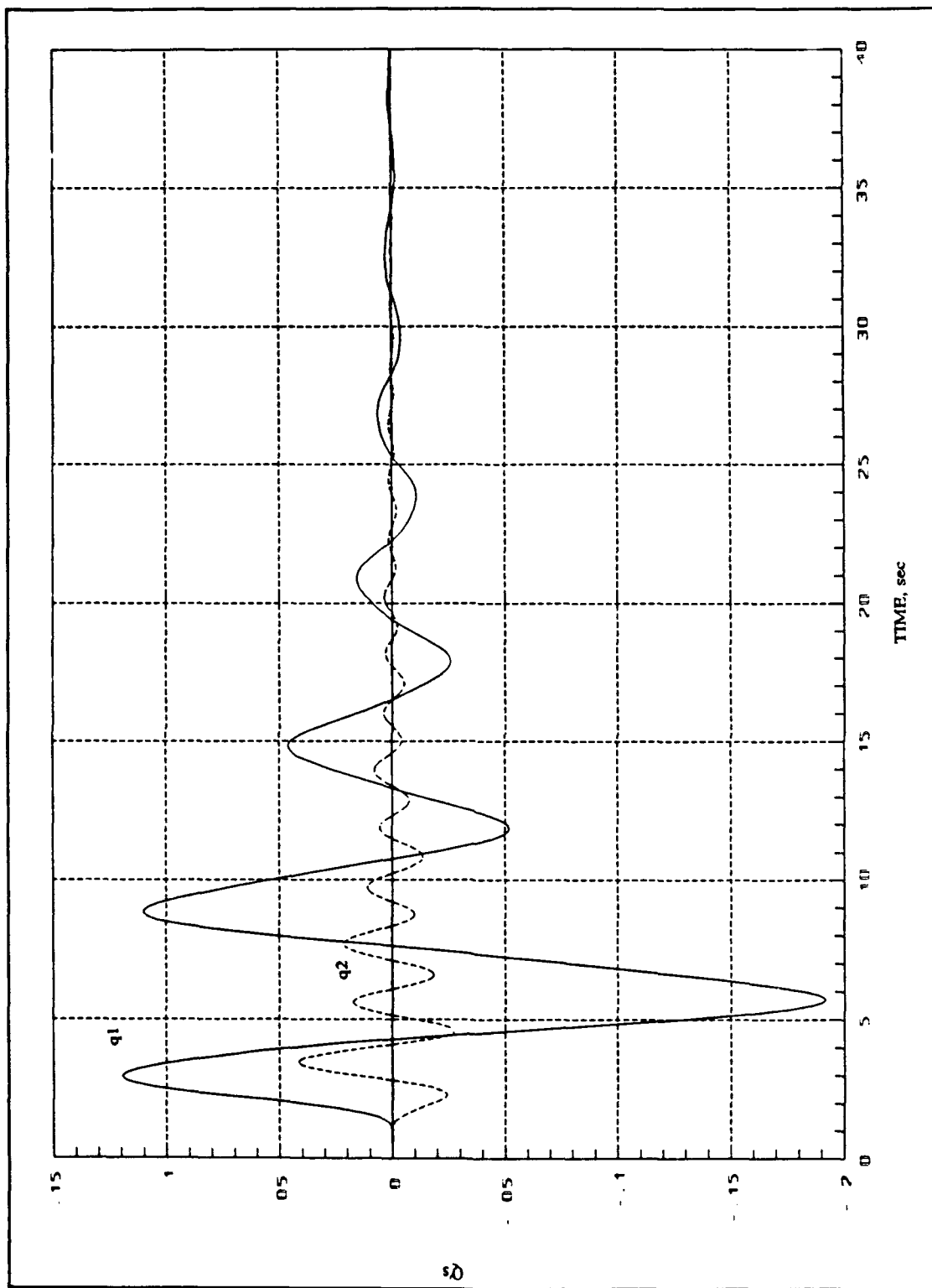


Figure 13 Simulated impulse response



**Figure 14** Modal amplitudes for the simulated slew maneuver





**Figure 15** Modal amplitudes for 0.5 N-m impulse response

maneuver. The impulse response shows that the amplitude of the first mode has increased but more importantly the second mode is proportionally greater when compared to the slew maneuver. This transient effect of the second mode dies out in about ten seconds, but the effect on the arm for those first ten seconds might present some problems, not the least of which could be damage to the sensitive piezoceramic sensors.

### **C. EXPERIMENTAL PROPORTIONAL-DERIVATIVE CONTROL**

In the first attempts to control the actual flexible system, several discoveries were made that required modification of the simulation and the software controller. The first discovery was the existence of the disturbance torque that was discussed in the previous section. The next discovery was the fact that the motor that drives the momentum wheel is capable of responding almost instantaneously to even large command inputs. Many safeguards had to be added to prevent damage to the system by the momentum wheel. It became clear that the motor had to be controlled very carefully from spin-up through control to spin-down. A separate control system was developed just to provide initial spin-up and final spin-down commands to the wheel. It was impossible to just provide a command to the wheel to speed up to 1000 RPM. The wheel would respond almost immediately and the torque developed would damage the flexible arm as well as the central air bearing aluminum diaphragms (consult [Ref. 2] for details on the air bearing). Instead, the control system is sent a series of small speed commands, issued every tenth of a second, to incrementally speed-up or speed-down the wheel in a controlled manner.

The control system diagram for the PD controller implemented is illustrated in Figure 16. The 30 degree slew maneuver that was performed is compared to the computer simulation of the flexible body. The block diagram of the control system is shown in Figure 16. Plots comparing the body position, Figure 17, body rate, Figure 18, wheel speed, Figure 19, and wheel torque, Figure 20. The results show very close correlation between the simulation and the experiment. In general the shapes of the responses mirror the simulation and the inflection points are almost collocated. It appears that the simplification of excluding the higher modes from the state-space model was a valid one.

One problem encountered was the reliability and sensitivity of the sensors in providing accurate feedback. The plots for the body rate and wheel torque display a great deal of noise. This can be attributed to the high noise levels encountered in the rate sensor. Similar noise was present in both the RVDT and wheel tachometer, but the application of an analog filter on the RVDT and a digital filter on the tachometer successfully removed the noise without introducing unreasonable delays. Attempts to filter the rate noise resulted in unacceptable delays in the control response and the signal had to be used as it was. It appears that a new sensor will be necessary to eliminate the noise problem.

Another condition that was discovered was the inability of the FSS to reach and maintain the desired equilibrium position. Because control of the wheel is only viable through impulse bits, the momentum wheel has a limited effect on the body over the impulse time bit that it acts over. Because of this, the exact time width and torque value

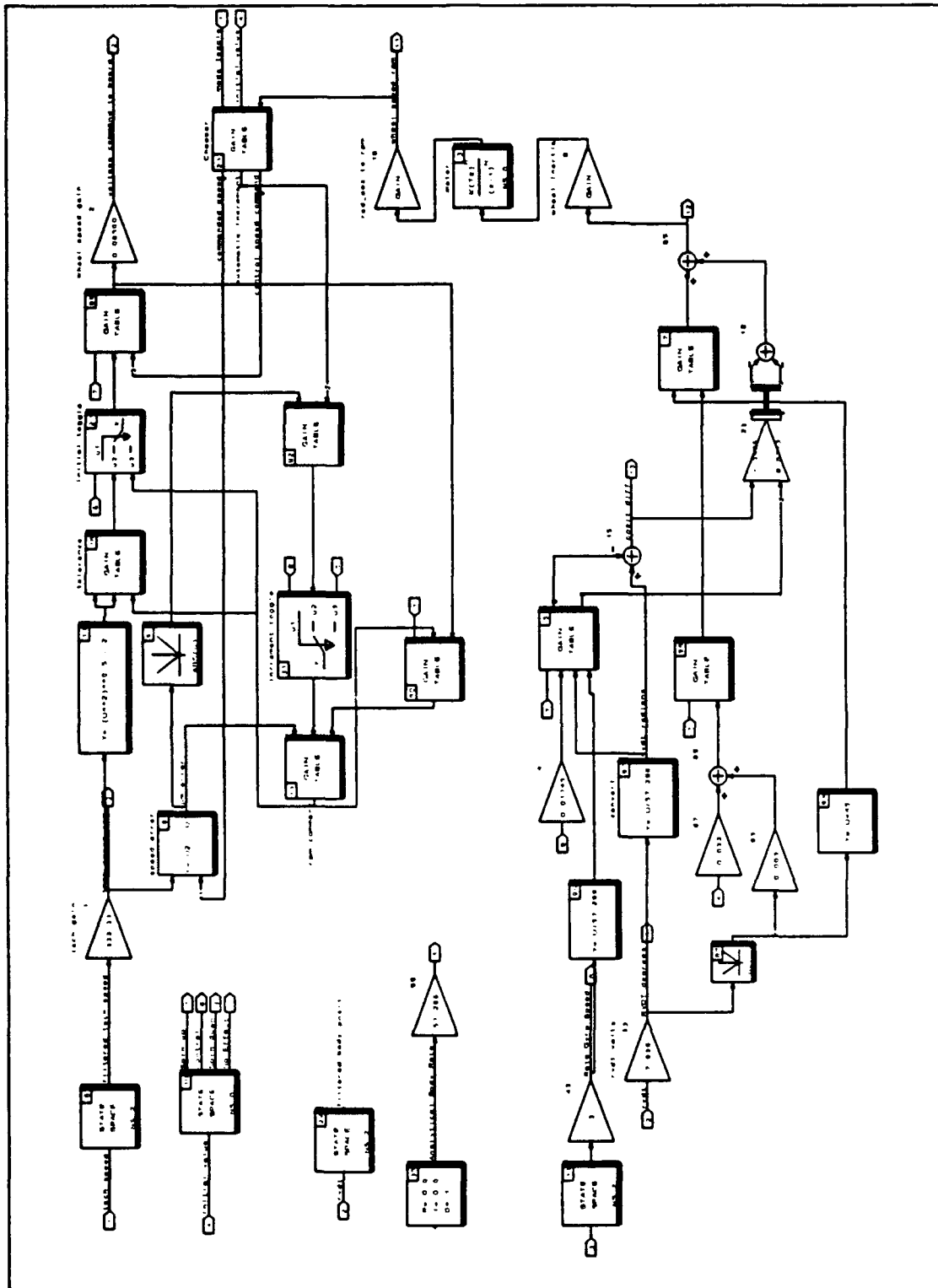


Figure 16 Block diagram for PD control system

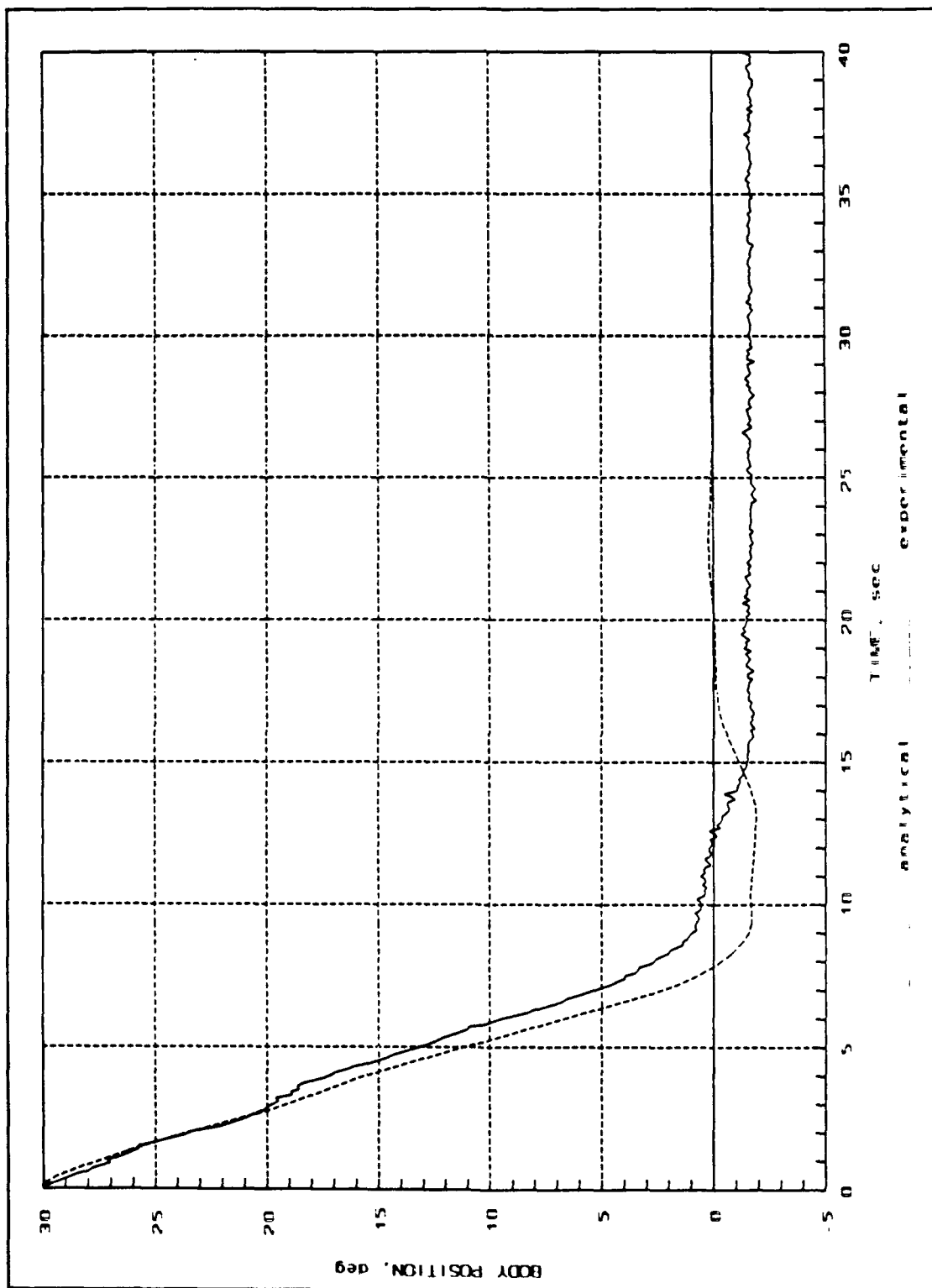


Figure 17 Body position comparison for 30 degree slew maneuver

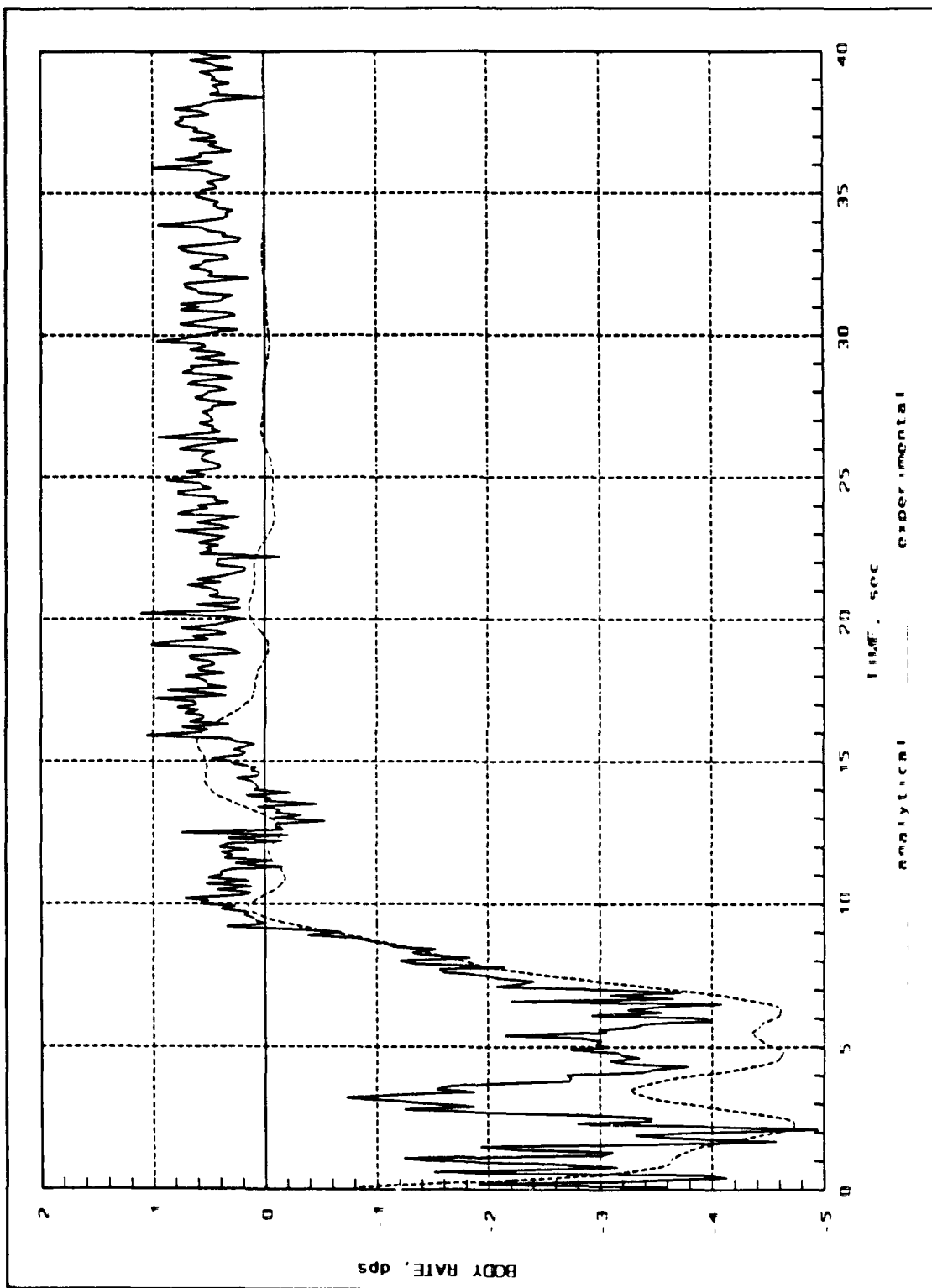


Figure 18 Body rate comparison for slew for 30 degree maneuver

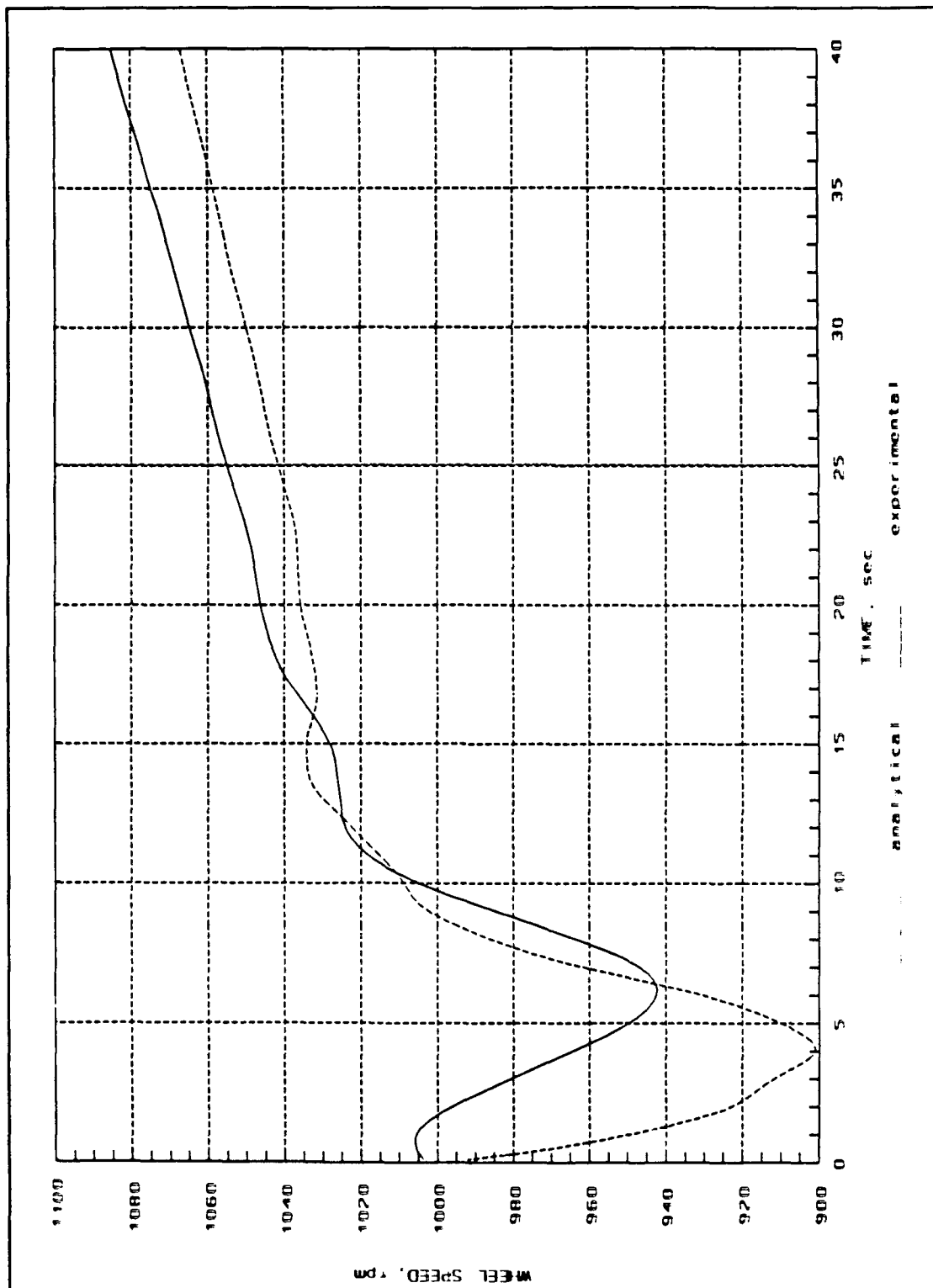


Figure 19 Momentum wheel speed comparison for 30 degree slew maneuver

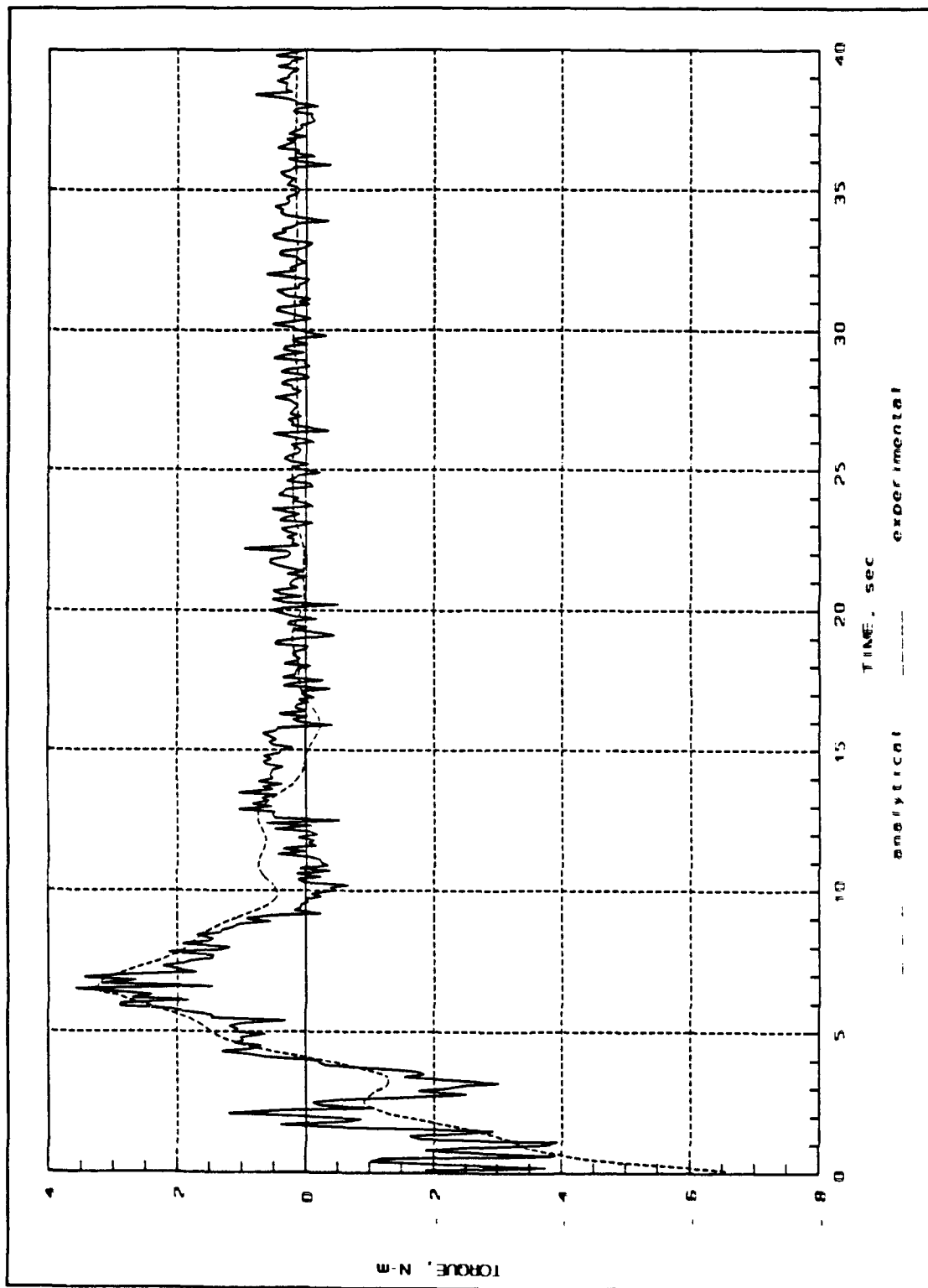


Figure 20 Wheel torque comparison for 30 degree slew maneuver



need to be tailored to achieve the desired position. When the impulse bit is too small, the wheel is unable to overcome the disturbance torque and the body settles short of its desired position. When the impulse bit is too large, the wheel over controls the body for the impulse period and the body settles above the desired position. With a few trials, the impulse bit was set to get the body to within 1.5 degrees of the desired position. Further refinement will take out this error.

## VI. CONCLUSIONS

The computer model of the Flexible Spacecraft Simulator that was developed by Watkins and Ward appears to closely approximate the physical model. A comparison of the body position, body rate and wheel speed data for both models show close correlation. It appears that truncation of the flexible modes beyond the first six does not degrade the computer model. The only major problem areas are the noisy rate sensor and the existence of the disturbance torque. The current plan is to replace the rate sensor with a lower noise model. The disturbance torque needs to be eliminated before a true "gravity free" environment can be achieved. One method that might alleviate the torque is to locate air sources on the central body and pass power and telemetry through a rotary couple.

The goal of developing and implementing an active damping system was only partially achieved. The control circuitry for the system has been built and tested. It performs as it was intended. Small input signals on the order of several volts are amplified by the circuit to the maximum desired control voltage range of  $\pm 175$  volts. There is a slight phase lag (about 30 degrees) between the actuator and sensor. It is believed that it results from the signal passing through the low pass filter. The major problem encountered involves the piezoceramic sensors and actuators. Of the four wafers that were bonded to the arm, only one is producing a reasonable output. It appears that either the wafers were not bonded uniformly or that the material properties

are not uniform (due to processing or damage after processing). A great deal of research must be completed into handling and bonding techniques to provide a more uniform product.

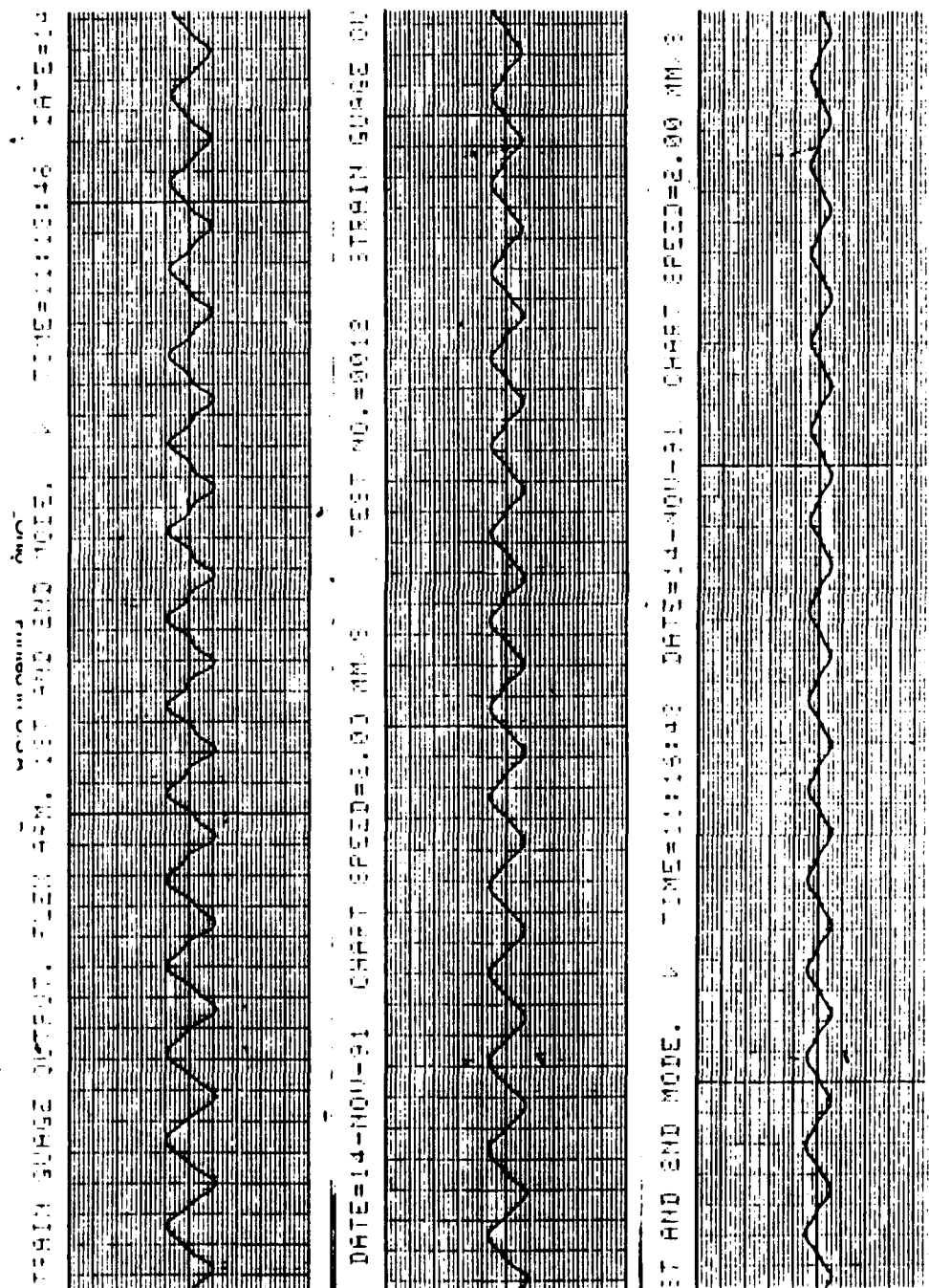
#### **A. RECOMMENDATIONS FOR FURTHER STUDY**

There is a great deal of work than can be done to provide active damping to the FSS. Obviously the first area of concern is the previously discussed problem with the consistency of the sensors and actuators. Once the simple system is operational further work can explore the effect of multiple sensors and actuators along the arm to truly tailor the response of the damping circuit to the maneuver being performed. Experimentation with a mix of collocated and nearly collocated sensors and actuators can be performed. Relative modal phasing techniques discussed in [Ref. 3] show great promise in simultaneously damping several modes at once.

A great deal of work can be put into developing methods to mechanically isolate the FSS from the overhead support beam to eliminate the disturbance torque. In the mean time, a more accurate model of that torque should be developed. Now that the basic system validity has been established, further work can be performed in exploring other control methods. Thrusters can be mounted onto the central body to provide control and desaturate the momentum wheel. The flexible arm can be removed and liquid tanks can be added to study the effects of liquid slosh. The flexible arm can be modified for studies in robotics. The adaptability of the FSS lends itself to a wide spectrum of research efforts.

## APPENDIX A

The following is a sample of the strip chart output for the damping measurements.



## APPENDIX B

### A. MSC/PAL 2 FINITE ELEMENT MODEL

#### TITLE FLEXIBLE ARM DESIGN

#### NODAL POINT LOCATIONS 1

1	0.0	0.0	0.0
2	0.057	0.0	0.0
3	0.6155	0.0	0.0
4	0.666	0.0	0.0
5	0.666	-0.0702	0.0
6	0.666	-0.6156	0.0
7	0.666	-0.6667	0.0
8	0.121	0.0	0.0
9	0.184	0.0	0.0
10	0.248	0.0	0.0
11	0.311	0.0	0.0
12	0.375	0.0	0.0
13	0.388	0.0	0.0
14	0.502	0.0	0.0
15	0.666	-0.1841	0.0
16	0.666	-0.2477	0.0
17	0.666	-0.3111	0.0
18	0.666	-0.3747	0.0
19	0.666	-0.4381	0.0
20	0.666	-0.5017	0.0

--BLANK LINE--

ZERO 1

TX 1

TY 1

TZ 1 2 3 4 5 6 7 8 9 10 11 12 13 14 15

TZ 16 17 18 19 20

RX 1 2 3 4 5 6 7 8 9 10 11 12 13 14 15

RX 16 17 18 19 20

RY 1 2 3 4 5 6 7 8 9 10 11 12 13 14 15

RY 16 17 18 19 20

RZ 1

--BLANK LINE--

MATERIAL 6.70E10 2.62E10 2.71E3 0.33 241E6 0.0 0.0

BEAM 2 1.5877E-3 0.0254 1.5877E-3 0.0254

CONNECT 1 TO 2

CONNECT 2 TO 8

BEAM 2 .05176 .0254 .05176 .0254

CONNECT 3 TO 4

CONNECT 4 TO 5

BEAM 2 .0947 .0254 .0947 .0254

CONNECT 6 TO 7

BEAM 2 1.5877E-3 0.0254 1.5877E-3 0.0254

CONNECT 5 TO 15

CONNECT 8 TO 9

CONNECT 9 TO 10

CONNECT 10 TO 11

CONNECT 11 TO 12

CONNECT 12 TO 13

CONNECT 13 TO 14

CONNECT 14 TO 3

CONNECT 15 TO 16

CONNECT 16 TO 17

CONNECT 17 TO 18

CONNECT 18 TO 19

CONNECT 19 TO 20

CONNECT 20 TO 6

MASS 7 .467

MASS 13 .467

MASS 5 .467

MASS 9 .467

MASS 10 .467

MASS 14 .467

MASS 3 .467

MASS 20 .467

MASS 6 .467

END DEFINITION

## B. FLEXIBLE ARM MODE SHAPES AND FREQUENCIES

MODE NO. 1 AT 1.39353E-01 CPS (8.75584E-01 RAD/SEC)

MODE	X TRANS	Y TRANS	Z TRANS	X ROT	Y ROT	Z ROT
1	0.0000E+0	0.0000E+00				
2	-1.7448E-08	-3.0363E-03	0.0000E+00	0.0000E+00	0.0000E+00	-1.0563E-01
3	-1.8841E-07	-2.9541E-01	0.0000E+00	0.0000E+00	0.0000E+00	-8.5835E-01
4	-1.8889E-07	-3.3876E-01	0.0000E+00	0.0000E+00	0.0000E+00	-8.5835E-01
5	-6.0256E-02	-3.3876E-01	0.0000E+00	0.0000E+00	0.0000E+00	-8.5835E-01
6	-6.0315E-01	-3.3876E-01	0.0000E+00	0.0000E+00	0.0000E+00	-1.0647E+00
7	-6.5756E-01	-3.3876E-01	0.0000E+00	0.0000E+00	0.0000E+00	-1.0647E+00
8	-3.7040E-08	-1.3420E-02	0.0000E+00	0.0000E+00	0.0000E+00	-2.1770E-01
9	-5.6325E-08	-3.0433E-02	0.0000E+00	0.0000E+00	0.0000E+00	-3.2130E-01
10	-7.5916E-08	-5.4183E-02	0.0000E+00	0.0000E+00	0.0000E+00	-4.1973E-01
11	-9.5201E-08	-8.3504E-02	0.0000E+00	0.0000E+00	0.0000E+00	-5.1004E-01
12	-1.1479E-07	-1.1891E-01	0.0000E+00	0.0000E+00	0.0000E+00	-5.9515E-01
13	-1.1877E-07	-1.2675E-01	0.0000E+00	0.0000E+00	0.0000E+00	-6.1163E-01
14	-1.5367E-07	-2.0426E-01	0.0000E+00	0.0000E+00	0.0000E+00	-7.4484E-01
15	-1.6259E-01	-3.3876E-01	0.0000E+00	0.0000E+00	0.0000E+00	-9.3551E-01
16	-2.2324E-01	-3.3876E-01	0.0000E+00	0.0000E+00	0.0000E+00	-9.7065E-01
17	-2.8574E-01	-3.3876E-01	0.0000E+00	0.0000E+00	0.0000E+00	-1.0000E+00
18	-3.5013E-01	-3.3876E-01	0.0000E+00	0.0000E+00	0.0000E+00	-1.0238E+00
19	-4.1564E-01	-3.3876E-01	0.0000E+00	0.0000E+00	0.0000E+00	-1.0419E+00
20	-4.8233E-01	-3.3876E-01	0.0000E+00	0.0000E+00	0.0000E+00	-1.0544E+00

MODE NO. 2 AT 4.19768E-01 CPS ( 2.63748E+00 RAD/SEC)

MODE	X TRANS	Y TRANS	Z TRANS	X ROT	Y ROT	Z ROT
1	0.0000E+0	0.0000E+00				
2	-1.1633E-07	9.5420E-03	0.0000E+00	0.0000E+00	0.0000E+00	3.2360E-01
3	-1.2562E-06	4.0008E-01	0.0000E+00	0.0000E+00	0.0000E+00	9.4715E-02
4	-1.2593E-06	4.0487E-01	0.0000E+00	0.0000E+00	0.0000E+00	9.4707E-02
5	6.6468E-03	4.0487E-01	0.0000E+00	0.0000E+00	0.0000E+00	9.4696E-02
6	-4.6923E-01	4.0487E-01	0.0000E+00	0.0000E+00	0.0000E+00	-1.3670E+00
7	-5.3909E-01	4.0487E-01	0.0000E+00	0.0000E+00	0.0000E+00	-1.3670E+00
8	-2.4695E-07	3.9768E-02	0.0000E+00	0.0000E+00	0.0000E+00	6.0683E-01
9	-3.7552E-07	8.4604E-02	0.0000E+00	0.0000E+00	0.0000E+00	8.0287E-01
10	-5.0614E-07	1.4014E-01	0.0000E+00	0.0000E+00	0.0000E+00	9.1895E-01
11	-6.3472E-07	1.9955E-01	0.0000E+00	0.0000E+00	0.0000E+00	9.5404E-01
12	-7.6533E-07	2.5965E-01	0.0000E+00	0.0000E+00	0.0000E+00	9.1096E-01
13	-7.9187E-07	2.7138E-01	0.0000E+00	0.0000E+00	0.0000E+00	8.9252E-01
14	-1.0245E-06	3.5870E-01	0.0000E+00	0.0000E+00	0.0000E+00	6.0093E-01
15	-1.4658E-02	4.0487E-01	0.0000E+00	0.0000E+00	0.0000E+00	-4.4768E-01
16	-5.1218E-02	4.0487E-01	0.0000E+00	0.0000E+00	0.0000E+00	-6.9543E-01
17	-1.0210E-01	4.0487E-01	0.0000E+00	0.0000E+00	0.0000E+00	-9.0310E-01
18	-1.6512E-01	4.0487E-01	0.0000E+00	0.0000E+00	0.0000E+00	-1.0720E+00
19	-2.3739E-01	4.0487E-01	0.0000E+00	0.0000E+00	0.0000E+00	-1.2012E+00
20	-3.1686E-01	4.0487E-01	0.0000E+00	0.0000E+00	0.0000E+00	-1.2915E+00

MODE NO. 3 AT 2.46305E+00 CPS ( 1.54758E+01 RAD/SEC)

MODE	X TRANS	Y TRANS	Z TRANS	X ROT	Y ROT	Z ROT
1	0.0000E+0	0.0000E+00				
2	-8.5620E-07	6.3049E-02	0.0000E+00	0.0000E+00	0.0000E+00	2.0593E+00
3	-9.2452E-06	3.0853E-02	0.0000E+00	0.0000E+00	0.0000E+00	-4.2843E+00
4	-9.2685E-06	-1.8550E-01	0.0000E+00	0.0000E+00	0.0000E+00	-4.2842E+00
5	-3.0076E-01	-1.8550E-01	0.0000E+00	0.0000E+00	0.0000E+00	-4.2842E+00
6	6.4868E-02	-1.8552E-01	0.0000E+00	0.0000E+00	0.0000E+00	4.6071E+00
7	3.0029E-01	-1.8552E-01	0.0000E+00	0.0000E+00	0.0000E+00	4.6071E+00
8	-1.8175E-06	2.4001E-01	0.0000E+00	0.0000E+00	0.0000E+00	3.2779E+00
9	-2.7639E-06	4.5463E-01	0.0000E+00	0.0000E+00	0.0000E+00	3.3494E+00

10	-3.7252E-06	6.4481E-01	0.0000E+00	0.0000E+00	0.0000E+00	2.4636E+00
11	-4.6715E-06	7.5787E-01	0.0000E+00	0.0000E+00	0.0000E+00	1.0847E+00
12	-5.6328E-06	7.7588E-01	0.0000E+00	0.0000E+00	0.0000E+00	-5.6260E-01
13	-5.8281E-06	7.6621E-01	0.0000E+00	0.0000E+00	0.0000E+00	-9.2674E-01
14	-7.5404E-06	4.9931E-01	0.0000E+00	0.0000E+00	0.0000E+00	-3.5500E+00
15	-6.6246E-01	-1.8550E-01	0.0000E+00	0.0000E+00	0.0000E+00	-2.0774E+00
16	-7.5629E-01	-1.8551E-01	0.0000E+00	0.0000E+00	0.0000E+00	-8.7814E-01
17	-7.7494E-01	-1.8551E-01	0.0000E+00	0.0000E+00	0.0000E+00	2.8353E-01
18	-7.2096E-01	-1.8551E-01	0.0000E+00	0.0000E+00	0.0000E+00	1.4059E+00
19	-5.9770E-01	-1.8551E-01	0.0000E+00	0.0000E+00	0.0000E+00	2.4732E+00
20	-4.0792E-01	-1.8551E-01	0.0000E+00	0.0000E+00	0.0000E+00	3.4842E+00

MODE NO. 4 AT 4.29463E+00 CPS ( 2.69839E+01 RAD/SEC)

MODE	X TRANS	Y TRANS	Z TRANS	X ROT	Y ROT	Z ROT
1	0.0000E+0	0.0000E+00				
2	-4.4690E-06	-6.8885E-02	0.0000E+00	0.0000E+00	0.0000E+00	-2.1933E+00
3	-4.8254E-05	1.4977E-01	0.0000E+00	0.0000E+00	0.0000E+00	-1.9775E+00
4	-4.8375E-05	4.9898E-02	0.0000E+00	0.0000E+00	0.0000E+00	-1.9776E+00
5	-1.3888E-01	4.9899E-02	0.0000E+00	0.0000E+00	0.0000E+00	-1.9777E+00
6	-2.9554E-02	4.9911E-02	0.0000E+00	0.0000E+00	0.0000E+00	1.0900E+01
7	5.2742E-01	4.9911E-02	0.0000E+00	0.0000E+00	0.0000E+00	1.0900E+01
8	-9.4867E-06	-2.4591E-01	0.0000E+00	0.0000E+00	0.0000E+00	-3.0573E+00
9	-1.4426E-05	-4.2201E-01	0.0000E+00	0.0000E+00	0.0000E+00	-2.2616E+00
10	-1.9444E-05	-5.0769E-01	0.0000E+00	0.0000E+00	0.0000E+00	-3.1088E-01
11	-2.4383E-05	-4.6347E-01	0.0000E+00	0.0000E+00	0.0000E+00	1.6121E+00
12	-2.9400E-05	-3.1472E-01	0.0000E+00	0.0000E+00	0.0000E+00	2.9278E+00
13	-3.0420E-05	-2.7541E-01	0.0000E+00	0.0000E+00	0.0000E+00	3.1152E+00
14	-3.9356E-05	8.5846E-02	0.0000E+00	0.0000E+00	0.0000E+00	2.5136E+00
15	-5.4382E-01	4.9901E-02	0.0000E+00	0.0000E+00	0.0000E+00	-4.5580E+00
16	-8.3782E-01	4.9903E-02	0.0000E+00	0.0000E+00	0.0000E+00	-4.5123E+00
17	-1.0951E+00	4.9904E-02	0.0000E+00	0.0000E+00	0.0000E+00	-3.4352E+00
18	-1.2526E+00	4.9906E-02	0.0000E+00	0.0000E+00	0.0000E+00	-1.3548E+00
19	-1.2474E+00	4.9907E-02	0.0000E+00	0.0000E+00	0.0000E+00	1.6738E+00
20	-1.0201E+00	4.9909E-02	0.0000E+00	0.0000E+00	0.0000E+00	5.6247E+00

MODE NO. 5 AT 6.85954E+00 CPS ( 4.30998E+01 RAD/SEC)

MODE	X TRANS	Y TRANS	Z TRANS	X ROT	Y ROT	Z ROT
1	0.0000E+0	0.0000E+00				
2	6.6667E-06	1.3416E-01	0.0000E+00	0.0000E+00	0.0000E+00	4.1530E+00
3	7.1976E-05	-1.9318E-01	0.0000E+00	0.0000E+00	0.0000E+00	6.4087E+00
4	7.2157E-05	1.3046E-01	0.0000E+00	0.0000E+00	0.0000E+00	6.4087E+00
5	4.4996E-01	1.3046E-01	0.0000E+00	0.0000E+00	0.0000E+00	6.4085E+00
6	-5.9894E-02	1.3054E-01	0.0000E+00	0.0000E+00	0.0000E+00	5.5237E+00
7	2.2237E-01	1.3054E-01	0.0000E+00	0.0000E+00	0.0000E+00	5.5237E+00
8	1.4152E-05	4.4476E-01	0.0000E+00	0.0000E+00	0.0000E+00	4.8565E+00
9	2.1520E-05	6.6554E-01	0.0000E+00	0.0000E+00	0.0000E+00	1.4838E+00
10	2.9005E-05	5.8657E-01	0.0000E+00	0.0000E+00	0.0000E+00	-3.9374E+00
11	3.6373E-05	2.1058E-01	0.0000E+00	0.0000E+00	0.0000E+00	-7.3832E+00
12	4.3857E-05	-2.7299E-01	0.0000E+00	0.0000E+00	0.0000E+00	-7.0899E+00
13	4.5377E-05	-3.6190E-01	0.0000E+00	0.0000E+00	0.0000E+00	-6.5626E+00
14	5.8707E-05	-7.1473E-01	0.0000E+00	0.0000E+00	0.0000E+00	1.1697E+00
15	6.8886E-01	1.3048E-01	0.0000E+00	0.0000E+00	0.0000E+00	-1.5049E+00
16	5.0573E-01	1.3049E-01	0.0000E+00	0.0000E+00	0.0000E+00	-4.0186E+00
17	2.0919E-01	1.3050E-01	0.0000E+00	0.0000E+00	0.0000E+00	-5.0945E+00
18	-1.1032E-01	1.3051E-01	0.0000E+00	0.0000E+00	0.0000E+00	-4.7066E+00
19	-3.5765E-01	1.3052E-01	0.0000E+00	0.0000E+00	0.0000E+00	-2.8528E+00
20	-4.4144E-01	1.3053E-01	0.0000E+00	0.0000E+00	0.0000E+00	4.5721E-01

MODE NO. 6 AT 1.28221E+01 CPS ( 8.05634E+01 RAD/SEC)

MODE	X TRANS	Y TRANS	Z TRANS	X ROT	Y ROT	Z ROT
1	0.0000E+0	0.0000E+00				
2	5.5373E-05	-1.6151E-01	0.0000E+00	0.0000E+00	0.0000E+00	-4.8114E+00
3	5.9758E-04	-4.5628E-01	0.0000E+00	0.0000E+00	0.0000E+00	9.8458E+00
4	5.9908E-04	4.0946E-02	0.0000E+00	0.0000E+00	0.0000E+00	9.8461E+00



5	6.9181E-01	4.0947E-02	0.0000E+00	0.0000E+00	0.0000E+00	9.8463E+00
6	-6.8019E-02	4.1036E-02	0.0000E+00	0.0000E+00	0.0000E+00	3.2250E+00
7	9.6778E-02	4.1036E-02	0.0000E+00	0.0000E+00	0.0000E+00	3.2250E+00
8	1.1755E-04	-4.8142E-01	0.0000E+00	0.0000E+00	0.0000E+00	-4.1161E+00
9	1.7875E-04	-5.5578E-01	0.0000E+00	0.0000E+00	0.0000E+00	2.7677E+00
10	2.4091E-04	-1.2091E-01	0.0000E+00	0.0000E+00	0.0000E+00	9.8123E+00
11	3.0208E-04	5.3246E-01	0.0000E+00	0.0000E+00	0.0000E+00	9.5185E+00
12	3.6422E-04	9.0264E-01	0.0000E+00	0.0000E+00	0.0000E+00	6.2103E-01
13	3.7684E-04	8.9258E-01	0.0000E+00	0.0000E+00	0.0000E+00	-2.2258E+00
14	4.8748E-04	-1.9173E-01	0.0000E+00	0.0000E+00	0.0000E+00	-1.0798E+01
15	1.2848E+00	4.0967E-02	0.0000E+00	0.0000E+00	0.0000E+00	8.6873E-01
16	1.2106E+00	4.0978E-02	0.0000E+00	0.0000E+00	0.0000E+00	-3.0173E+00
17	9.2997E-01	4.0989E-02	0.0000E+00	0.0000E+00	0.0000E+00	-5.5874E+00
18	5.3562E-01	4.1000E-02	0.0000E+00	0.0000E+00	0.0000E+00	-6.5145E+00
19	1.4257E-01	4.1011E-02	0.0000E+00	0.0000E+00	0.0000E+00	-5.5588E+00
20	-1.2773E-01	4.1022E-02	0.0000E+00	0.0000E+00	0.0000E+00	-2.6055E+00

## APPENDIX C

### PROGRAM FORME

C

C AUTHOR: R. J. WATKINS

C

C MODIFIED: E. S. JONES

C DATE: MAY 18, 1991

C MODIFIED: NOVEMBER 6, 1991

C

C THIS PROGRAM READS IN DATA GIVEN BY GIFTS OUTPUT AND

C PUTS IT INTO A FORMAT FOR STATE-SPACE MODELING

C

CHARACTER\*80 DUMMY

DOUBLE PRECISION A(16,16), B(16), AI, BI

REAL OMEGA(6),U(6,20),V(6,20),PSX(20),PSY(20),MS(20),IZZO1

1,DS(6), ES(6), FS(6), GS(6), IW, IZZO2,HS(6),JS(6)

OPEN (UNIT=10, FILE='EVANMODE.TXT', STATUS='OLD')

OPEN (UNIT=11, FILE='PSE.DAT',STATUS='OLD')

OPEN (UNIT=12, FILE='MSE.DAT',STATUS='OLD')

OPEN (UNIT=13, FILE='CHECKE.DAT',status='new')

OPEN (UNIT=14, FILE='ADMPE',status='new',CARRIAGECONTROL='LIST')

```

OPEN (UNIT=15, FILE='BDMPE',status='new',CARRIAGECONTROL='LIST')
OPEN (UNIT=16, FILE='ECHOE',status='new')

C
C  READ IN OUTPUT FROM EVANMODE.TXT (FEM SHAPE OUTPUT)
C
C
7 FORMAT (/ ,40X,E11.5,/)
13 FORMAT (6X,E11.4,1X,E11.4)

DO 2 I=1,6
    READ(10,7) OMEGA(I)
    WRITE(16,7) OMEGA(I)
    DO 6 J=1,20
        READ(10,13) U(I,J),V(I,J)
        WRITE(16,7) U(I,J),V(I,J)
    6  CONTINUE
2  CONTINUE

C
C  READ IN MSE AND PSE DATA FILES
C  PSE IS POSITION OF EACH NODE (SUBBODY) IN METERS
C  AND MSE IS THE MASS OF EACH SUBBODY IN KG. NOTE 1: FIRST
C  ENTRY IN MSE.DAT IS THE INERTIA TERM FOR THE SYSTEM (IZZ01)
C  NOTE 2: MASS AND POSITION OF EACH NODE MUST BE IN SAME
C  SEQUENCE AS OUTPUT IN PR_OUT FILE!!

```

C

DO 20 I=1,20

READ (11,\*) PSX(I), PSY(I)

20 CONTINUE

READ (12,\*) IZZO1

DO 30 I=1,20

READ (12,\*) MS(I)

30 CONTINUE

C

C FORM THE TERMS FOR THE A AND B MATRIX. ALSO CALCULATE

C CHECK MATRIX ES: ALL ENTRIES SHOULD BE APPROX 1 IF

C DATA INPUT CORRECTLY. OUTPUT IS IN CHECK.DAT (ASCII)

C INPUT DAMPING FOR ARM (ZETA) NOTE: COULD BE CHANGED

C TO VECTOR IF NECESSARY

C

ZETA=0.004

IZZO2=IZZO1

DO 35 I=1,6

DS(I)=0.0

ES(I)=0.0

DO 32 J=1,20

DS(I)=DS(I)+(V(I,J)\*PSX(J)-U(I,J)\*PSY(J))\*MS(J)

ES(I)=ES(I)+(U(I,J)\*\*2+V(I,J)\*\*2)\*MS(J)

```

32    CONTINUE

      WRITE(13,*) ES(I)

      IZZO2=IZZO2-DS(I)**2

35    CONTINUE

      DO 38 I=1,6

        FS(I)=DS(I)*OMEGA(I)**2

        GS(I)=(OMEGA(I)**2)*IZZO2+DS(I)*FS(I)

        HS(I)=2.0*OMEGA(I)*ZETA*DS(I)

        JS(I)=2.0*ZETA*OMEGA(I)*IZZO2+DS(I)*HS(I)

38    CONTINUE

C
C  FORM A AND B MATRIX
C

      DO 45 I=1,14

        DO 42 J=1,14

          A(I,J)=0.0

42    CONTINUE

45    CONTINUE

      DO 50 I=1,7

        A(I,I+7)=1.0

50    CONTINUE

      DO 57 I=2,7

        A(8,I)=FS(I-1)/IZZO2

```

57 CONTINUE

DO 65 I=9,14

DO 60 J=2,7

$A(I,J) = -DS(I-8) * FS(J-1) / IZZO2$

60 CONTINUE

DO 63 J=9,14

$A(I,J) = -DS(I-8) * HS(J-8) / IZZO2$

63 CONTINUE

$A(I,I) = -JS(I-8) / IZZO2$

$A(8,I) = HS(I-8) / IZZO2$

$A(I,I-7) = -GS(I-8) / IZZO2$

65 CONTINUE

C

C FORM CONTROL INPUT MATRIX B

C

DO 70 I=1,7

$B(I) = 0.0$

70 CONTINUE

$B(8) = 1.0 / IZZO2$

DO 75 I=9,14

$B(I) = -DS(I-8) / IZZO2$

75 CONTINUE

C

```
C  WRITE MATRIX TO FILES. USE MATRIXX SUBROUTINE MATSAV TO
C  CONVERT DATA INTO READABLE FORM FOR MATRIXX.  OUTPUT
C  IS IN Admp AND Bdmp.
C
C
      CALL MATSAV(14,'ASYS',16,14,14,0,A,AI,'(1P2E24.15)')
      CALL MATSAV(15,'BSYS',16,14,1,0,B,BI,'(1P2E24.15)')
C
C  END OF PROGRAM
C
      STOP
      END
```

## REFERENCES

1. Ward, Christina C., *Attitude Control of Flexible Structures*, Master's Thesis, Naval Postgraduate School, Monterey, California, September 1990.
2. Watkins, R. Joseph Jr., *The Attitude Control of Flexible Spacecraft*, Master's Thesis, Naval Postgraduate School, Monterey, California, June 1991.
3. Betros, Robert S. and Bronowicki, Allen J., "Seminar Notes," *Active Damping Workshop*, Spring, 1991.
4. *Guide to Modern Piezoelectric Ceramics*, Vernitron Corporation, Bedford, Ohio.
5. Shields, John Potter, *Basic Piezoelectricity*, Howard W. Sams & Co., 1966.



### INITIAL DISTRIBUTION LIST

- |    |  |   |
|----|--|---|
| 1. | Defense Technical Information Center<br>Cameron Station<br>Alexandria, Virginia 22304-6145   | 2 |
| 2. | Library, Code 52<br>Naval Postgraduate School<br>Monterey, California 93943-5002   | 2 |
| 3. | Chairman, Code AA<br>Department of Aeronautics and Astronautics<br>Naval Postgraduate School<br>Monterey, California 93943                     | 1 |
| 4. | Chairman, Code SP<br>Department of Aeronautics and Astronautics<br>Naval Postgraduate School<br>Monterey, California 93943                     | 1 |
| 5. | Professor Brij N. Agrawal, Code AA/Ag<br>Department of Aeronautics and Astronautics<br>Naval Postgraduate School<br>Monterey, California 93943 | 2 |
| 6. | Professor I. M. Ross, Code AA/Ro<br>Department of Aeronautics and Astronautics<br>Naval Postgraduate School<br>Monterey, California 93943      | 1 |
| 7. | LT Evan S. Jones, USN<br>12217 Cedar Ridge Dr. NE<br>Albuquerque, NM 87112   | 2 |